1994

Spectroscopic characterization of hypericin and related compounds

Jeanne Lenore Wynn
Iowa State University

Order Number 9518458

Spectroscopic characterization of hypericin and related compounds

Wynn, Jeanne Lenore, Ph.D.

Iowa State University, 1994

U·M·I
300 N. Zeeb Rd.
Ann Arbor, MI 48106

Spectroscopic characterization of hypericin and

related compounds

by

Jeanne Lenore Wynn

A Dissertation Submitted to the

Graduate Faculty in Partial Fulfillment of the

Requirements for the Degree of

DOCTOR OR PHILOSOPHY

Department: Chemistry
Major: Analytical Chemistry

Approved:

Signature was redacted for privacy.

In Charge of Major Work

Signature was redacted for privacy.

For the Major Department

Signature was redacted for privacy.

For the Graduate College

Iowa State University
Ames, Iowa

1994

To Him who created all things
visible and invisible, and
who is able to do immeasurably more
than all we ask or imagine

TABLE OF CONTENTS

GENERAL INTRODUCTION

Hypericin is a multi-ring quinone compound that exhibits a variety of photodynamic effects.[1-4] One of these effects that has been of particular interest recently is its antiviral activity. Several studies have determined that the presence of light is important for the antiviral activity of hypericin.[5-8]. However, the mechanism of action for hypericin is unknown. Several mechanisms have been proposed including singlet oxygen formation, superoxide radicals, and excited state proton transfer.[9-11]. Before a complete understanding of the mechanism of action is possible, the relevant chemical, physical and biological properties of hypericin must be established.

The research for this dissertation involved physical characterization of hypericin. Three studies were undertaken. The first involved a study of the aggregation states of hypericin in a variety of solvents. In addition Raman spectroscopy was employed to corroborate the assigned electronic transition dipoles. The second study involved the use of surface enhanced resonance Raman spectroscopy to investigate the chromophore of the bio-organism *Stentor coeruleus*. The chromophore of *Stentor* is structurally very similar to hypericin. Three protein complexes from *Stentor* were studied in order to elucidate structural information about the chromophores. The third study investigated the feasibility of using Langmuir-Blodgett techniques to obtain ordered monolayers of hypericin. The effect of subphase composition was also investigated. Absorption and Raman spectroscopies were used to characterize the Langmuir-Blodgett films.

Dissertation Organization

This dissertation is arranged in the format where papers that have been or will be submitted to journals are included. Following the General Introduction and Dissertation Organization sections, short backgrounds on Raman spectroscopy and Langmuir Blodgett films are presented. References for the General Introduction section follow immediately. The first paper has been submitted to the *Journal of Physical Chemistry*. T. M. Cotton is the co-author. The second paper has been submitted to *Journal of Physical Chemistry*. The other authors for this paper are T. M. Cotton, P.-S. Song, J. H. Kim, R. Dai and N.-B. Tao. The third paper is written in a format for *Langmuir*. A General Summary concludes the dissertation.

Raman Spectroscopy

Background

The Raman effect was first observed by Indian physicist C. V. Raman in 1928. He noted that a small fraction of the radiation scattered by certain molecules was different in wavelength from that of the incident beam. He also observed that these wavelength shifts were dependent upon the chemical structure of the molecule responsible for the scattering. The first twenty years after its discovery, there was a great deal of interest in the use of Raman spectroscopy for chemical structure studies. However, the rapid development of commercial infrared (IR) spectrometers resulted in a decrease of activity in the field of Raman spectroscopy. It was not until the application of the He-Ne laser to Raman spectroscopy in 1963 that interest was renewed. Today, Raman instrumentation is equal to or in some cases better than IR instrumentation.[12,13]

Basic Theory

When light passes through a sample, the electric field of the electromagnetic wave interacts with the electrons of the sample. This results in some of the incident radiation being scattered in all directions. The frequency of most of this scattered radiation is unchanged from that of the incident light. This is known as Rayleigh scattering. However, a small percentage of the scattered light is scattered at a different frequency. This is Raman scattering. If the light is scattered at frequency lower than that of the incident light, it is called Stokes Raman scattering, whereas light scattered at a higher frequency is known as anti-Stokes Raman scattering. The intensity of the Raman light is very weak, typically about 10^6 times weaker than the intensity of the Rayleigh scattered light. The difference in frequency between the incident and scattered radiation corresponds to vibrational energy levels of the molecule responsible for the scattering. Raman scattering is manifested by a change in a molecule from its initial vibrational state to a different vibrational state.[12,14,15]

The interaction of light with a molecule can cause the electron cloud of the molecule to oscillate at the same frequency as the incident light. The extent to which this occurs depends upon the polarizability (α) of the electron cloud. This distortion of the electron cloud is known as the induced dipole moment (μ), and can be defined in classical terms as

$$\mu = \alpha E \qquad (1)$$

where E is the electric field and α is the polarizability. Since E is time dependent and the polarizability varies with internuclear distance, equation 1 can be expanded to give the classic Raman equation

$$\mu = \alpha_o E_o \cos 2\pi \nu t + \frac{1}{2} E_o Q_o \frac{\partial \alpha}{\partial Q} [\cos 2\pi t(\nu+\nu_\upsilon) + \cos 2\pi t(\nu-\nu_\upsilon)] \qquad (2)$$

where α_o is the equilibrium polarizability, E_o is the amplitude of the wave, υ is the frequency of the light, t is time, Q_o is the maximum vibronic amplitude, and υ_υ is the vibrational frequency of the molecule. The first term of this equation represents Rayleigh scattering, the second term Stokes Raman scattering, and the third term anti-Stokes Raman scattering.[14,16] From this equation it can be seen that when $\partial\alpha/\partial Q \neq 0$, Raman scattering occurs. This is a fundamental requirement for Raman scattering; a change in polarizability must occur during a molecular vibration in order for that vibration to be Raman active.

Although equation 2 predicts the existence of both Stokes and anti-Stokes scattering, it does not predict the intensity differences observed between the two. At room temperature the Stokes lines are much more intense than the anti-Stokes lines. A quantum mechanical treatment can account for this difference, which is the result of Boltzmann distribution of state populations. In other words, at room temperature, most molecules are in the lowest vibronic level of the ground electronic state. After undergoing Raman scattering, these molecules will be in an excited vibrational state. This results in the more intense Stokes Raman scattering.

Raman spectroscopy has recently been applied to many biological systems.[14,17,18] Raman spectroscopy has several advantages over the use of infrared spectroscopy for the study of biological molecules. One advantage is that water can be used as a solvent because it is a poor Raman scatterer. This allows biological systems to be studied *in vivo*. Another advantage is that special optics and sample holders are not necessary because Raman excitation lines are in the ultraviolet or visible regions. A third advantage is that the use of lasers as an excitation source make it possible to study very small sample sizes. One major disadvantage of Raman spectroscopy is the inherent weakness of the Raman scattering signal. Also, in many cases fluorescence can completely obscure the Raman signal. Two methods that have been employed to overcome the low signal intensity of the Raman signal are resonance Raman spectroscopy and surface enhanced Raman spectroscopy. Both of these techniques are discussed briefly below.

Resonance Raman

Resonance Raman scattering refers to the technique where the excitation wavelength lies within an electronic absorption band of the molecule. The intensity of some of the Raman peaks can be enhanced 10^2 to 10^6 times over normal Raman intensities. The resonance Raman effect is the result of the promotion of an electron into an excited electronic state followed by immediate relaxation into a ground vibrational state. The emission process is essentially instantaneous. The use of resonance Raman simplifies the Raman spectra because not all normal Raman bands are enhanced equally. The strongest enhancement occurs only for those vibrations that undergo a large change

in equilibrium geometry upon electronic excitation. Only those vibrational modes that are totally symmetric or the modes that couple the ground and excited electronic states are enhanced. These two classes of enhancement are called A-term and B-term enhancement respectively. The vibrational frequencies observed for resonance Raman scattering are ground state frequencies of the molecule.[19]

Resonance Raman is very useful for the study of structure and function relationships of biological chromophores. The use of resonance Raman allows the vibrational modes of the chromophore to be selectively enhanced. In this way, detailed information about the chromophore can be obtained with little or no interference from the surrounding protein structures.

One major drawback to the use of resonance Raman spectroscopy is interference often encountered from fluorescence. Fluorescence appears as a broad background signal that often completely obscures the Raman signal. One technique that has been employed to overcome this problem is surface enhanced resonance Raman spectroscopy.

Surface Enhanced Raman Spectroscopy

Raman scattering and resonance Raman have also been used to study molecules adsorbed on metal surfaces. Surface enhanced Raman spectroscopy (SERS) is both a sensitive and selective technique. Metal surfaces can enhance the Raman signal up to 10^7 times.[20] At the same time, scattering from solvents or solution species is relatively weak. Another major advantage of SERS is that the fluorescence of the adsorbed molecule is often quenched, allowing the Raman signal to be easily observed. From equation (1), it can be seen that the enhancement of the Raman signal at metal surfaces can result from

two different mechanisms. These are an electromagnetic field effect and a chemical interaction mechanism. In the electromagnetic mechanism it is proposed that a large increase in the electric field (E) experienced by an adsorbate at a metal surface. In the chemical enhancement theory it is proposed that there are perturbations of the polarizability (α) from the interactions of molecules with the surface. Both mechanisms have been found to contribute to the increase in Raman signal observed for molecules adsorbed at metal surfaces, although the relative contribution of each effect is still under much debate.[18,20]

The most common metals for SERS experiments are silver, gold and copper. Enhancement has also been observed for other metals that are highly reflective in the visible region including lithium, potassium and sodium.[21] SERS substrates are typically either electrochemically roughened electrodes, metal colloids or vacuum deposited island films. Each type of substrate has its own advantages as well as disadvantages. Electrodes can be used to control the potential at the surface. Colloids are very easy to prepare but suffer from instability and variation from one preparation to the next. Island films can be prepared with excellent reproducibility and great purity, but sometimes produce poorer enhancements than colloids and electrodes.[22]

Langmuir-Blodgett Films

Background

The term Langmuir film refers to a film of insoluble molecules at a gas-liquid (typically air-water) interface. When these films are transferred from the air-water interface to a solid substrate they are called Langmuir-Blodgett films. The history of

monolayer films is often traced back to the ancient Babylonians. The Babylonians would use the spreading pattern of oil on a water surface to forecast future events. It is generally agreed that the first scientific attempt to study molecular films was by Benjamin Franklin in 1757. Franklin documented the calming effect that a teaspoon of oil had on a windswept pond. Lord Rayleigh is credited with the concept of films that are only a single molecule in thickness. In 1891, Agnes Pockels developed a method of manipulating oil film at the air-water interface. This method is the model for today's monolayer instrumentation. Irving Langmuir, considered the father of the field, carried out the first systematic studies of monolayers of amphiphilic molecules at the air-water interface and as a result laid much of the foundation for the field of monolayer films. Katherine Blodgett demonstrated the construction of ordered multilayers by successive deposition of monolayer films onto solid substrates.[23-25] Today, Langmuir-Blodgett films are used as model systems and for fundamental research.

Experimental

The Langmuir-Blodgett experiment is conceptually very simple. A small quantity of an appropriate solution is spread on the surface of a liquid subphase, typically water. After the solvent has evaporated, the monomolecular layer is compressed until a quasi-solid layer is formed that is one molecule thick . A substrate is then dipped through the subphase to transfer the monolayer. Multilayer films can be built up by repeatedly passing the substrate through the monolayer film.[26] Of course, there are some practical considerations that must be made for each of these steps.

Film Spreading The most common method of dispersing a substance at the air-water interface is to dissolve the molecule of interest in a spreading solvent. An ideal spreading solvent should be pure and chemically inert with respect to both the film material and the subphase. It should evaporate in a reasonable period of time (a few minutes) and it should be insoluble in the subphase. In addition, the spreading solvent must dissolve a reasonable amount of the film forming material. Concentrations of 0.1-1 mg/mL are typical. The most commonly used spreading solvents are chloroform, cyclohexane and hexane. For materials that are insoluble in these solvents, a mixed solvent system may be used. Methanol-chloroform or acetone-hexane are two of the more common systems. The spreading solution is usually delivered dropwise to the water surface with a microliter syringe or pipet.[23]

The Subphase The most common subphase is water. However, other materials such as mercury and glycerol have also been used.[24] The water must be extremely pure and the surface is usually aspirated to remove any dust or other contamination immediately prior to spreading the monolayer.

Troughs and Barriers The trough that contains the subphase and the barriers are usually made of teflon. Teflon is chosen because it is hydrophobic, oleophobic, resistant to most chemical and easily machined. Unfortunately it is also porous and can pick up contaminants easily. Therefore great care must be taken to ensure cleanliness. Most troughs are either rectangular or circular in geometry and have one fixed and one movable barrier. There are many different designs for movable barriers, but all designs must ensure that there is a good seal between the movable barrier and the edge of the

trough. This is necessary to prevent leakage of the monolayer. Most modern day troughs are also thermostated to allow the temperature of the subphase to be accurately controlled within a few tenth of a degree. Trough volumes can range from 0.2 to 5 L.[24,25]

Film Deposition Most Langmuir-Blodgett depositions involve hydrophilic substrates such as glass, quartz, or silicon wafers.[24] As with all materials used in monolayer work, the substrates must be scrupulously cleaned. There are two methods of transferring films from the air-water interface to a substrate, vertical deposition and the horizontal lifting method. Vertical deposition is the more conventional of the two and was first demonstrated by Blodgett and Langmuir.[24] For this method the substrate is raised or lowered through the air-water interface while a constant surface pressure is maintained. Each subsequent pass through the interface can transfer another monolayer onto the substrate resulting in well ordered multilayers. The horizontal transfer method involves lowering a horizontal substrate until it just touches the water surface. The substrate is held in this position long enough for the monolayer to spread and equilibrate (typically a few seconds) and then removed.[23]

The Pressure-Area Isotherm

The most commonly measured property of a monolayer at the air-water interface is the surface pressure. This measurement is presented as a pressure-area isotherm where the surface pressure is plotted versus the area occupied by the molecular film. The surface pressure (Π) is actually a measurement of the difference between the surface tension of pure water and that of the water covered with a molecular film. The most common way to measure surface pressure is with a Wilhelmy balance. The Wilhelmy

balance detects surface pressure changes by the vertical displacement of a thin suspended plate partially immersed in the subphase. The plate is usually a completely wet piece of filter paper or a thin slide of glass or platinum[23,24].

The pressure-area isotherm contains information about the stability of the monolayer at the air-water interface, the orientation of molecules, phase transitions, and conformational changes. An isotherm can contain four distinct regions. The initial portion of the curve, where the area per molecule is large, is called the "gas" phase. In this region the surface pressure is very low and there are no interactions between the individual molecules on the surface layer. As the film is compressed, the intermolecular distances become smaller and the surface pressure starts to increase. The pressure in this region of the isotherm usually increases with some curvature, with a slope somewhat steeper than the gaseous region. This region of the isotherm is termed the "liquid" state or the liquid-expanded state. This state is not observed for all molecules. When the barrier is compressed even further, the molecules reach a point where they are in their nearly closest packed arrangement. This is called the "solid" state or the liquid-condensed state. The pressure-area plots at this point are nearly straight and very steep. If the monolayer is compressed even further, it will reach a pressure where it will collapse. Usually a sharp decrease in pressure is observed, although the isotherm for some larger molecules may just exhibit a decrease in slope. This is a very simplified version of the pressure-area isotherm. Often the liquid-expanded region of the isotherm can consist of a variety of phases such as orientationally disordered (liquid-expended), orientationally ordered (liquid-condensed) and striped.[23,24]

Besides pressure-area isotherms there are many other techniques used to characterize monolayers. These techniques include optical, electrochemical and microscopy techniques. They will not be discussed here but are thoroughly reviewed elsewhere.[23,24,27]

References

(1) Pace, N.; Mackinney, G. *J. Am. Chem. Soc.* **1941,** *63,* 2570.

(2) Giese, A. C. In *Photophysiology Current Topics in Photobiology and Photochemistry,* Vol VI, Giese, A.C., Ed.; Academic Press: New York, 1971; 77.

(3) Knox, J. P.; Dodge, A. D. *Plant Cell Environ.* **1985,** *8,* 19.

(4) Durán, N.; Song, P.-S. *Photochem. Photobiol.* **1986,** *43,* 677.

(5) Carpenter, S.; Kraus, G. A. *Photochem. Photobiol.* **1991,** *53,* 169.

(6) Hudson, J. B.; Lopez-Bazzocchi, I.; Towers, G. H. N. *Antivir. Res.* **1991,** *15,* 101.

(7) Lopez-Bazzocchi, I.; Hudson, J. B.; Towers, G. H. N. *Photochem. Photobiol.* **1991,** *54,* 95.

(8) Degar, S.; Prince, A. M.; Pascual, D.; Lavie, G.; Levin, B.; Mazur, Y.; Lavie, D.; Ehrlich, L. S.; Carter, C.; Meruelo, D. *Aids Res. Hum. Retroviruses* **1992,** *8,* 1929.

(9) Heitz, J. R. In *Light Activated Pesticides,* Heitz, J. R.; Downum, K. R., Eds.; American Chemical Society: Washington D.C., 1987; 38.

(10) Knox, J. P.; Samuels, R. I.; Dodge, A. D. In *Light Activated Pesticides,* Heitz J. R.; Downum, K. R., Eds.; American Chemical Society: Washington DC, 1987; 265.

(11) Gai, F.; Fehr, M. J.; Petrich, J. W. *J. Am. Chem. Soc.* **1993,** *115,* 3384.

(12) Grasselli, J. G.; Snavely, M. K.; Bulkin, B. J. *Chemical Applications of Raman Spectroscopy*, John Wiley and Sons: New York, 1981.

(13) Durig, J. R.; Sullivan, J. F. In *Physical Methods of Chemistry, 2nd Ed. Vol IIIA*, Rossiter, B. W.; Hamilton, J. F., Eds.; John Wiley and Sons: New York, 1987; 1.

(14) Tu, A. T. *Raman Spectroscopy in Biology: Principles and Applications*, John Wiley and Sons: New York, 1982.

(15) Lambert, J. B.; Shurvell, H. F.; Verbit, L.; Cooks, R. G.; Stout, G. H. *Organic Structural Analysis*, Macmillan Publishing Co., Inc: New York, 1976.

(16) Colthup, N. B.; Daly, L. H.; Wiberley, S. E. *Introduction to Infrared and Raman Spectroscopy*, 3rd Ed, Academic Press: Boston, 1990.

(17) Spiro, T. G. *Biological Applications of Raman Spectroscopy*, Vol 3, John Wiley and Sons: New York, 1988.

(18) Cotton, T. M. In *Spectroscopy of Surfaces*, Clark, R. J.; Hester, R. E. Eds.; John Wiley and Sons: New York, 1988, 91.

(19) Morris, M. D.; Wallen, D. J. *Anal. Chem.* **1979,** *51*, 182A.

(20) Garrell, R. L. *Anal. Chem.* **1989,** *61*, 401A.

(21) Campion, A. In *Vibrational Spectroscopy of Molecules on Surfaces*, Yates, J. T.; Madey, T. E. Eds.; Plenum Press: New York, 1987, 345.

(22) Cotton, T. M.; Kim, J.-H.; Chumanov, G. D. *J. Raman. Spec.* **1991,** *22*, 729.

(23) Gaines, G. L. *Insoluble Monolayers at Liquid-Gas Interfaces*, Interscience Publishers: New York, 1966.

(24) Ulman, A. *An Introduction to Ultrathin Organic Films From Langmuir-Blodgett to Self Assembly,* Academic Press: Boston, 1991.

(25) Roberts, G. *Langmuir-Blodgett Films,* Plenum Press: New York, 1990.

(26) Vincent, P. S.; Barlow, W. A.; Boyle, F. T.; Finney, J. A. *Thin Solid Films,* **1979,** *60,* 265.

(27) Kuhn, H.; Möbius, D.; Bücher, H. In *Physical Methods of Chemistry, Part IIIB,* Weisberger, A.; Rossiter, B. W. Eds.; Wiley Interscience: New York, 1972, 577.

SPECTROSCOPIC PROPERTIES OF HYPERICIN IN SOLUTION AND AT SURFACES

A paper submitted to the *Journal of Physical Chemistry*

Jeanne L. Wynn and Therese M. Cotton

Abstract

The absorption and fluorescence spectra of hypericin were studied in a wide variety of organic solvents. Three distinct types of hypericin absorption spectra were observed and are representative of hypericin in monomeric, aggregated and protonated states. The solvatochromatic shifts of monomeric hypericin were also investigated. These shifts are related to the solvent's hydrogen bonding donor ability for protic solvents and to the solvent's polarizability and hydrogen bonding acceptor ability for aprotic solvents. In addition, the surface enhanced resonance Raman scattering (SERRS) spectra of neutral hypericin, protonated hypericin and deprotonated hypericin were studied in order to corroborate previously assigned electronic transition dipoles. The SERRS data support the assignment of the the S_1 transition as polarized through the short axis of the hypericin skeleton and the S_2 transition as polarized through the carbonyl axis of molecule.

Introduction

Hypericin (Figure 1), a multi-ring aromatic quinoidal compound, is known to exhibit a variety of photodynamic effects.[1-4] The hypericin pigment is found in certain species of plants from the genus *Hypericum*, the most common of which is Saint John's wort.[5] Ingestion of hypericin containing plants by grazing animals has been shown to cause hypericism, a condition of severe sensitivity to light.[1,6-7] This photosensitizing effect

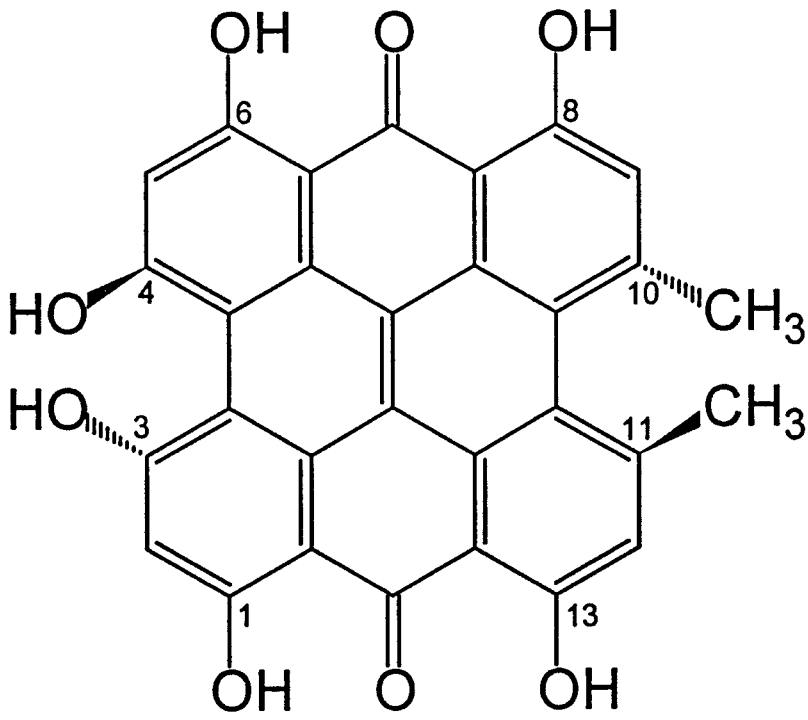

Figure 1. Structure of hypericin.

results is severe skin irritation, high body temperatures, and in extreme cases death of the animal. Hypericin and similar pigments were also found in some Australian insects and in the protozoan *Stentor coeruleus*.[4] *Stentor* was shown to exhibit both a step-up photophobic response and a negative phototactic behavior in the presence of light.[8] The chromophore of *Stentor* is stentorin. Stentorin is the photoreceptor believed to be responsible for the organisms extreme sensitivity to solar radiation and is structurally very similar to hypericin.[9] Hypericin has also been used as an anti-depressant and is known to have bactericidal and other physiological properties.[4]

Recently, hypericin was demonstrated to be a potent antiviral agent.[10] It was shown to inhibit both the replication and the infection cycles of several retroviruses, including the LP-BM5 virus, the Friends leukemia virus and the human immunodeficiency virus.[11] In several studies, the role of light in the viral inactivation process was investigated.[12-15] Carpenter and Kraus[12] found that the antiviral activity of hypericin was completely dependent on the presence of light for the inactivation of equine infectious anemia virus. Hudson *et al.*[13] found that the presence of light was not necessary for antiviral activity but that the light did substantially enhance the antiviral activity of hypericin against murine cytomegalovirus and Sinbis virus. Degar *et al.*[15] also found light to substantially enhance the antiviral activity of hypericin against HIV.

Several mechanisms have been proposed for the photodynamic activity of hypericin, including a Type I mechanism involving superoxide radical formation, a Type II mechanism is which singlet oxygen is formed and an excited state proton release mechanism.[16] Hypericin was shown to produce singlet oxygen on exposure to light[3,4,17]

and stentorin was shown to photogenerate enough singlet oxygen to kill *Stentor*.[18] The singlet oxygen quantum yield was determined to be 0.73.[19] In addition, singlet oxygen participates in the hypericin promoted inhibition of succinoxidase in mitochondria.[20] Evidence for the photogeneration of superoxide by hypericin was also observed.[17,21,22] Investigations of *Stentor coeruleus* support a light induced pH change across the cell membrane, suggesting that a proton release is the primary photoprocess responsible for its photodynamic action.[8,23,24] Recently, ground and excited state pK_a values were determined for hypericin in two different studies, pK_a = 11.0, 11.3 and pK_a^* = 9.8, 12.2.[25,26] The first deprotonation step has been assigned to position 3. Ground and excited state pK_a values for the protonation of one of the carbonyl sites also were determined, pK_a = -6.0, pK_a^* = -3.2.[25]

In order to understand more fully the photodynamic mechanism of hypericin, it is first necessary to establish its relevant physical, chemical, and biological properties. Absorption and fluorescence spectra of hypericin were previously reported in several solvents.[1,8,27-29] Yamazaki *et al.*[26] studied the absorption and fluorescence spectra of hypericin in several organic solvents of varying degrees of polarity. In addition, they report spectra in aqueous solutions of different pH. Phosphorescence[30], Raman[31], NMR[32,33], EPR[21,34], IR[9] and transient absorption spectra[35] were also reported for hypericin. This physical data is important for correlating the molecular structure of hypericin with its biological activity.

Aggregation of dye molecules or chromophoric species has been found to be an important factor in the area of photodynamic therapy.[36] The formation of aggregates can

drastically alter the absorption and fluorescence spectrum of a molecule by causing spectral band shifts, deviations from Beer's Law, and fluorescence quenching at high concentrations. The presence of aggregates can modify photophysical properties, which in turn may affect the ability of a molecule to function as a photosensitizer. Aggregation is dependent upon several factors including the structure of a molecule, its concentration, the solvent, the temperature, and the presence of electrolytes. Many mechanisms have been proposed to explain the association of molecules in solution some of which are additive forces of a van der Waals type, intermolecular hydrogen bonding, hydrogen bonding with the solvent and coordination with metal ions.[37]

Hypericin is reported to be monomeric in ethanol and acetone solutions, and to form large unstructured aggregates in aqueous solution.[8,31] Yamazaki *et al.*[26] reported hypericin to be monomeric in all of the organic solvents that they examined. In this study, the absorption and fluorescence spectra of hypericin at various concentrations was measured in a wide range of solvents in order to explore further the aggregation behavior of hypericin in solution. Raman spectroscopy was also employed to support the previously assigned electronic transitions of hypericin.

Material and Methods

The hypericin used in this study was obtained from LC Services Corporation, Woburn, Massachusetts. The purity of the hypericin was reported to be at least 98%. The purity was tested using thin layer chromatography (TLC). Sigma TLC precoated silica plates with fluorescent indicator were used. The mobile phase was toluene, butanol and formic acid 6:4:0.15. Only one spot was obtained and the sample was used without

further purification. Absolute ethanol (200 proof) was obtained from Midwest Grain. The methanol, acetonitrile, ethyl acetate, THF and hexane were HPLC grade solvents purchased from Fisher. Acetone and dimethylformamide were Aldrich HPLC grade solvents. The benzyl alcohol and acetic acid were Aldrich reagent grade. The lactic acid was reagent grade from Baker. All other solvents were Fisher reagent grade. The chloroform and carbon tetrachloride were passed through basic alumina columns to remove any stabilizers or other impurities. All other solvents were used without further purification.

All solutions were prepared from a stock solution of 3.8×10^{-4} M hypericin in absolute ethanol. The stock solution was stored in the dark at -15°C. The solutions containing one solvent were initially prepared by drying an aliquot of the hypericin stock solution under nitrogen and then adding the solvent of interest to the dry film. The solutions in ether and dioxane required sonication (Cole Parmer model 8851) for approximately three to five minutes to completely solubilize the film. Serial dilutions were then performed on these solutions for the concentration studies. The mixed solvent systems were prepared by slowly adding the solvent of interest to an aliquot of the hypericin stock solution. During the addition of the solvent, the mixture was gently agitated by hand to ensure complete mixing.

Absorption spectra were obtained using a Perkin Elmer Lambda 6 spectrophotometer. All spectra were obtained at a scan rate of 600 nm/min, a slit width of 1 nm and were background corrected. The fluorescence excitation and emission spectra were obtained using a Spex Fluoro Max. The fluorescence spectra were detected

perpendicular to the excitation source, and were corrected for variation in lamp intensity, and detector response. Excitation and emission slits were 1 mm wide.

Surface enhanced resonance Raman scattering (SERRS) spectra were collected using a Spex Triplemate spectrometer with a Princeton Instruments CCD detector (model LN1152) cooled to -120°C. A Coherent Ar^+ 200 series laser and a Coherent Kr^+ 100 series laser were used as the excitation sources. The laser power at the sample was approximately 10 mW and scattered radiation was collected in a backscattered configuration. Vacuum deposited silver island films were used as the SERRS substrate. The films were prepared by depositing 50 Å of silver onto clean glass slides at a rate of 0.2 Å/s. The slides were dipped in 4×10^{-6} M hypericin solutions for ten minutes, removed from solution, rinsed with deionized water, and placed in an optical dewar containing liquid nitrogen.

Results

Hypericin is sparingly soluble in most solvents. It forms a red solution in most organic solvents, a green solution in basic media, and violet dispersions of fine particles in water. The absorption spectrum of hypericin in neutral organic solvents contains two major visible transitions $S_0 \rightarrow S_1$ (λ_{max} = 500 - 600 nm) and $S_0 \rightarrow S_2$ (λ_{max} = 485 - 425 nm), and two major UV bands. The redmost transition has been assigned to the first π to π^* transition that is polarized along the short axis of the hypericin skeleton.[26] The first transition contains three vibronic levels each of which is split into two levels.[30] For hypericin in ethanol, these are represented by the absorption bands at 591 nm (v = 0), 547 nm (v = 1), and 510 nm (v = 2). The splitting of these levels can be seen as

shoulders on the 591 nm and 547 nm peaks. Because the 510 nm peak is very weak, no shoulder is observed. The second transition, $S_0 \rightarrow S_2$, is the transition polarized along the long axis of the hypericin skeleton that contains the carbonyl groups.[26]

The absorption maxima for hypericin in various solvents are presented in Table 1. The spectra obtained in acetone and ethanol were found to be in agreement with previous results with respect to peak shape and position.[1,8,27-29] The position of the redmost peak was also in agreement with the results of Yamazaki *et al.*[26] for methanol, acetonitrile and tetrahydrofuran.

Three distinct types of absorption spectra were obtained for hypericin and an example of each is shown in Figure 2. The first type of spectrum, designated Type I, occurs in most organic solvents including acetone, acetonitrile, THF, dioxane, dimethylformamide and alcohols. Type I spectra are characterized by the dominance of the redmost band. In a given solvent, no changes were observed in the absorption spectra over the concentration range studied (10^{-4} M to 10^{-8} M). For Type I spectra, the peak maxima of both the first ($S_0 \rightarrow S_1$) and the second ($S_0 \rightarrow S_2$) electronic transitions were found to shift with solvent. However, the positions of the UV peaks did not vary as much with solvent.

The second type of spectrum (Type II) was obtained in acidic solvents including concentrated sulfuric acid, acidic ethanol, ether, lactic acid, acetic acid and formic acid. These spectra also did not show any concentration dependent spectral changes over the range studied (10^{-5} M to 10^{-8} M). Type II spectra differ from Type I in several ways. First, except for concentrated sulfuric acid, the redmost peaks are blue shifted and more

TABLE 1: Absorption maxima for hypericin in various solvents

Solvent	Absorption maxima (nm)									
Tetrahydrofuran	600		555	516	482		385	339	286	
Dimethylformamide	598		554	515	482		386			
Benzyl Alcohol	596		551	515	480		390	335		
Acetone	596		551	514	477					
Acetonitrile	594		550	512	478		384	336	286	
Butanol	592		549	511	476		385	333	286	
Ethyl Acetate	592		549	511	477		384	334	285	
Ethanol	591		547	510	475		382	332	285	
Dioxane	590		547	510	471			330	283	
Methanol	588		545	509	471		384	328	282	
Conc H_2SO_4	650		597		500			325	238	220
Lactic Acid	581	569	540	504	455	433		320		
Ethanol + H^+	581	569	539	504	454	430		321	280	
Ether	580	569	540	507	452	428		326	280	230
Acetic Acid	579	567	538	503	453	430		320	279	
Formic Acid	578		537	501	454	432		321	279	
Cyclohexane	613		570		484			332	289	
Hexane	613		570		486			333	292	
Toluene	609		570		481			331		
Carbon tetrachloride	609		568		479		395	330	286	
Water	598		560					324	285	
Chloroform	595		570		484		397	330	286	

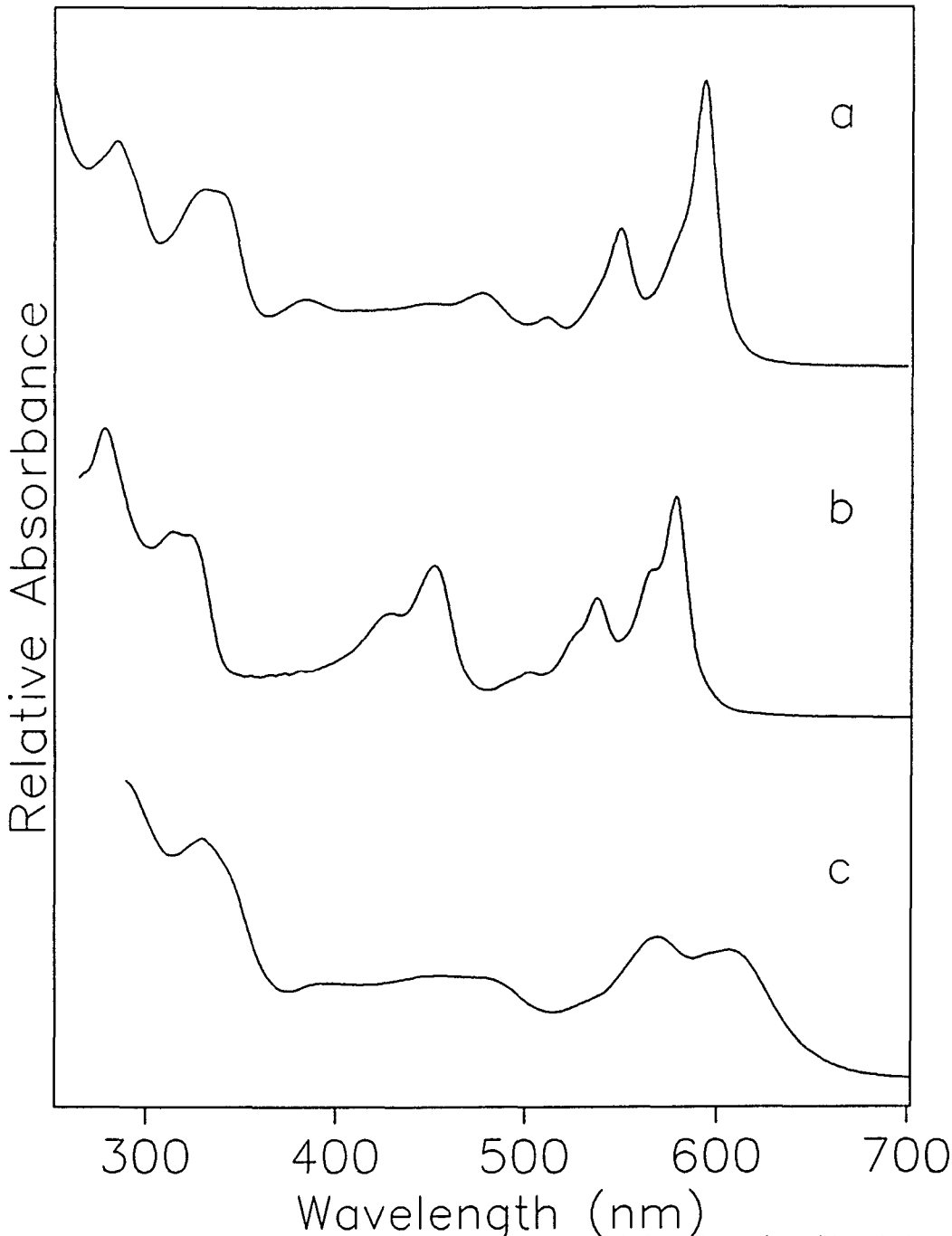

Figure 2. Absorption spectra of hypericin in a) acetonitrile, b) acetic acid and c) toluene. The concentration of hypericin was 3.8×10^{-6} M for acetonitrile and acetic acid and 3.8×10^{-5} M for toluene. Scan rate were 600 nm/min, slit width = 1 nm, path length = 1 cm.

vibronic structure is observed. For the concentrated sulfuric acid solution, the visible peaks are very red shifted and little vibronic structure is observed. Second, in the acidic solvents, the S_2 transition normally around 475 nm is blue shifted to ca. 455 nm and the transition is much more intense. Third, a slight hyperchromism is observed in the UV region. Again, the peak positions in the visible region are more affected by solvent than those in the UV. The spectra obtained in ether also exhibited a shoulder at 598 nm indicating a fraction of the hypericin is present in solution as the Type I species. When the solution of hypericin in acidic ethanol is neutralized with base, the absorption spectrum reverts back to the hypericin in ethanol Type I spectrum.

The third type (Type III) of spectrum is obtained in water and in non-polar organic solvents such as toluene, carbon tetrachloride, chloroform, hexane and cyclohexane. Hypericin is very insoluble in all of these solvents, and hence it must be added from an ethanol solution in order to solubilize a measurable amount. The percentage of ethanol used to solubilize the hypericin in nonpolar solvents is critical. If the concentration of ethanol is too high, the absorption spectrum begins to resemble that of hypericin in pure ethanol. For hexane, a concentration of ethanol as low as 1% was sufficient to produce bands characteristic of an ethanol type spectrum (see Figure 3). All of the solutions used in this study were prepared with 0.5% of ethanol and 99.5% of the solvent of interest. Type III spectra exhibit large reductions in extinction coefficients across both the visible and ultra-violet spectral regions, and a reduction in the overall oscillator strength also occurs. Type III spectra also exhibit changes in the relative intensity of the peaks associated with the S_1 transition. For water, cyclohexane, and toluene, the first (v=0)

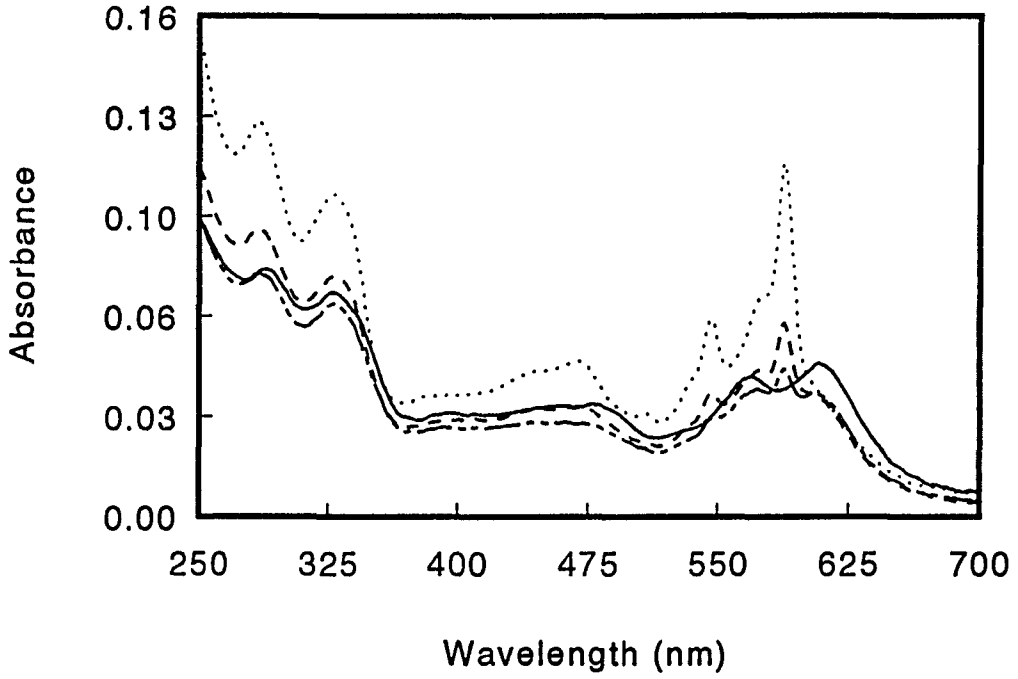

Figure 3. Absorption spectra of hypericin in mixed solvent system, hexane/ethanol. (——) 99.5% v/v hexane, (— ·· —) 99.0% hexane, (– – –) 98.75 % hexane, (·····) 97.5% hexane. The concentration of hypericin was 3.8×10^{-6} M.

peak is no longer the most intense peak of the transition. The peak for the v=1 transition becomes the most intense. For hexane, chloroform and carbon tetrachloride, these two peaks are nearly equal in intensity. Another characteristic of the Type III spectra is that the visible bands become much broader and less vibronic structure is observed. The relative absorbance of bands in the UV region is also increased dramatically compared to the red region. The spectra of hypericin in these solvents do not appear to change with concentration. However due to the large decrease in extinction coefficient, concentrations below 10^{-6} M could not be studied.

The spectrum of hypericin in aqueous sulfuric acid (not shown) resembles both Type II and Type III spectra. The band positions are similar to those of hypericin in pure water. A decrease in the extinction coefficient and broad bands are also observed. However the relative intensity of the S_2 absorption band is much greater than that observed for a Type III spectrum. The intensity is of the same magnitude as that of the S_1 absorption bands. This combination type spectrum was observed for concentrations of sulfuric acid ranging from 10^{-5} M to 9 M. Above 9 M the spectrum resembles the Type II spectrum of hypericin in concentrated sulfuric acid, with the redmost band at 650 nm.

Fluorescence emission and excitation spectra were also obtained for hypericin in the same solvents. The emission maxima are presented in Table 2. For all emission spectra, the maximum of the second vibronic peak (i.e. 547 nm for ethanol) was used as the excitation wavelength. Typical emission spectra for each of the three types of absorption spectra are presented in Figure 4. The emission spectra for both Type I and Type II are the expected mirror image of the lowest energy absorption transition. The emission

TABLE 2: Fluorescence emission maxima for hypericin in various solvents

Solvent	Emission maxima (nm)		
Tetrahydrofuran	602	652	709
Dimethylformamide	601	651	708
Benzyl Alcohol	601	650	704
Acetone	599	648	704
Acetonitrile	596	644	700
Butanol	596	644	700
Ethyl Acetate	597	644	696
Ethanol	594	642	698
Dioxane	591	641	696
Methanol	592	640	694
Conc H_2SO_4	662	719	
Lactic Acid	585	631	685
Ethanol + H^+	582	630	684
Ether	599	648	705
Acetic Acid	582	629	682
Formic Acid	585	631	685
Cyclohexane	593	643	670
Hexane	593	642	
Toluene	596	645	701
Carbon tetrachloride	595	643	
Water	598	649	
Chloroform	599	648	700

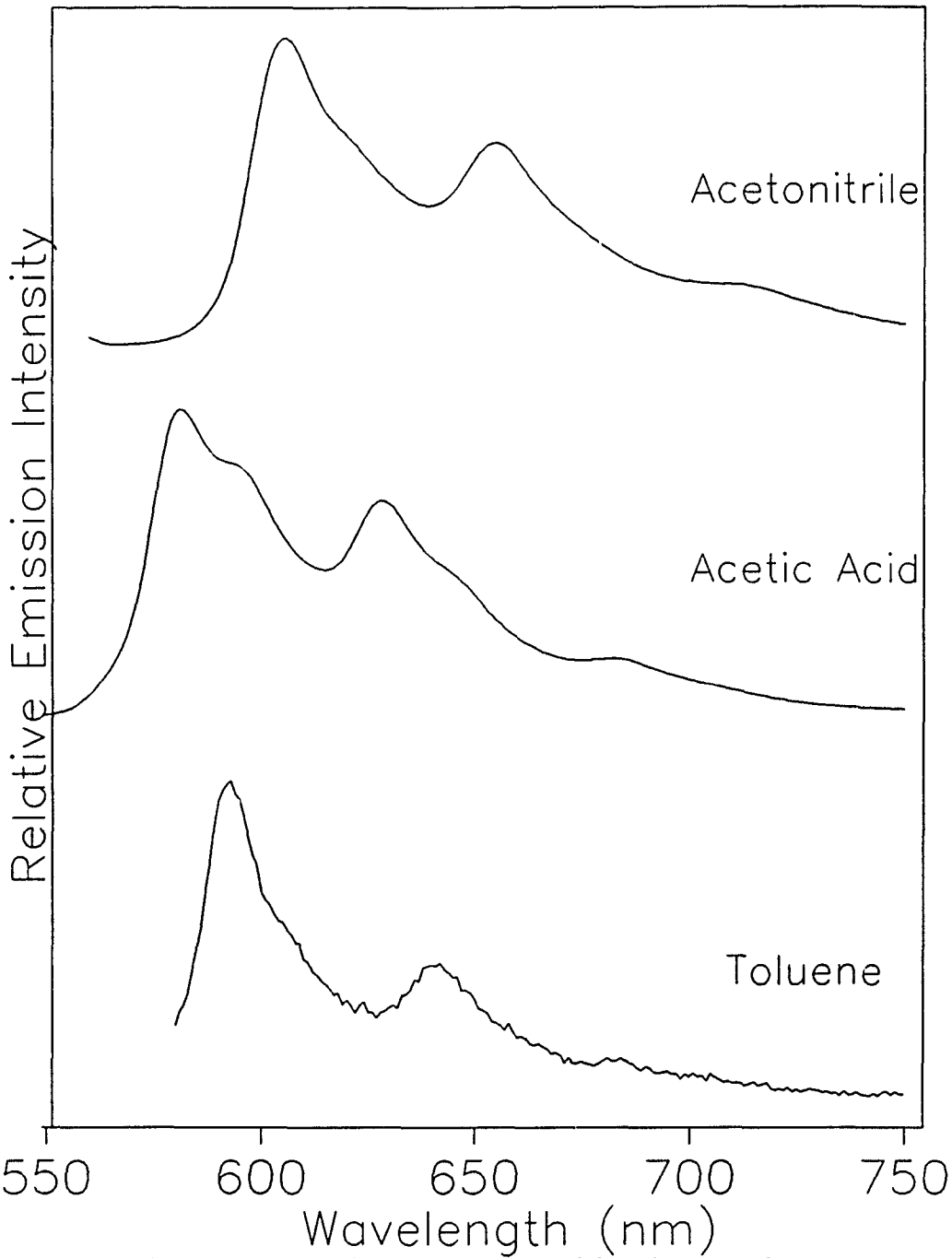

Figure 4. Fluorescence emission spectra of hypericin. Concentrations are the same as for Fig. 2. λ_{ex}: acetonitrile = 550 nm, acetic acid = 567 nm, toluene = 570 nm. Sample interval = 1 nm, integration time = 0.1 s, and slit widths = 1 mm.

intensity of hypericin in all of the Type III solutions was very weak, and the fluorescence spectrum resembled that of hypericin in ethanol. Emission spectra were also studied as a function of concentration. Both the relative intensity of the fluorescence peaks and their positions vary with hypericin concentration. Results for hypericin in acetonitrile are presented in Figure 5.

Excitation spectra were also obtained for all solutions and an example of each type of spectrum is presented in Figure 6. The fluorescent emission peak maximum was used as the emission wavelength. The excitation spectra for hypericin in the solvent systems of Type I and Type II correlate very well with the absorption spectra. The excitation spectra for the Type III spectra resembled that of ethanol for all solvents except that for carbon tetrachloride which resembled acidic ethanol. Excitation spectra were also studied as a function of concentration and did not change except at high concentrations (10^{-4} M) where spectral distortions occur because of self-absorption.

Resonance Raman spectroscopy was used in this study to corroborate the electronic assignments. Resonance Raman is a very useful and sensitive tool for probing specific electronic transitions to detect changes in molecular structure along an electronic transition dipole. For this study, SERRS was used instead of conventional resonance Raman spectroscopy. The resonance Raman scattering signal for hypericin is very weak especially in the low frequency region, and the intense fluorescence of hypericin interferes with the Raman signal. The use of surface enhanced Raman provides a much stronger signal and the hypericin fluorescence is quenched by the metal surface. The spectra obtained for hypericin at silver surfaces were shown to be very similar to the

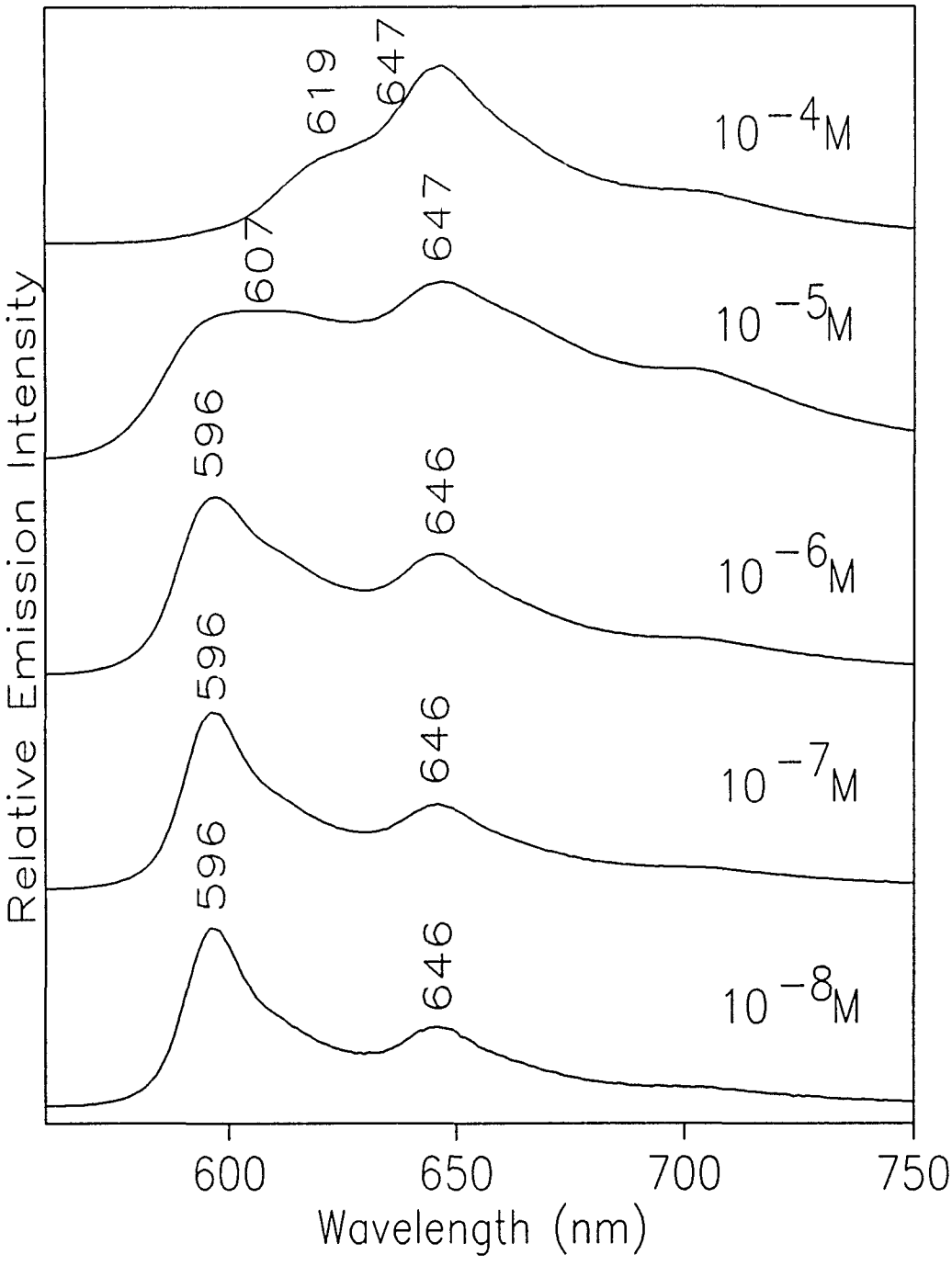

Figure 5. Fluorescence emission spectra of different concentrations of hypericin in acetonitrile. λ_{ex} = 550 nm. Other experimental conditions same as Figure 4.

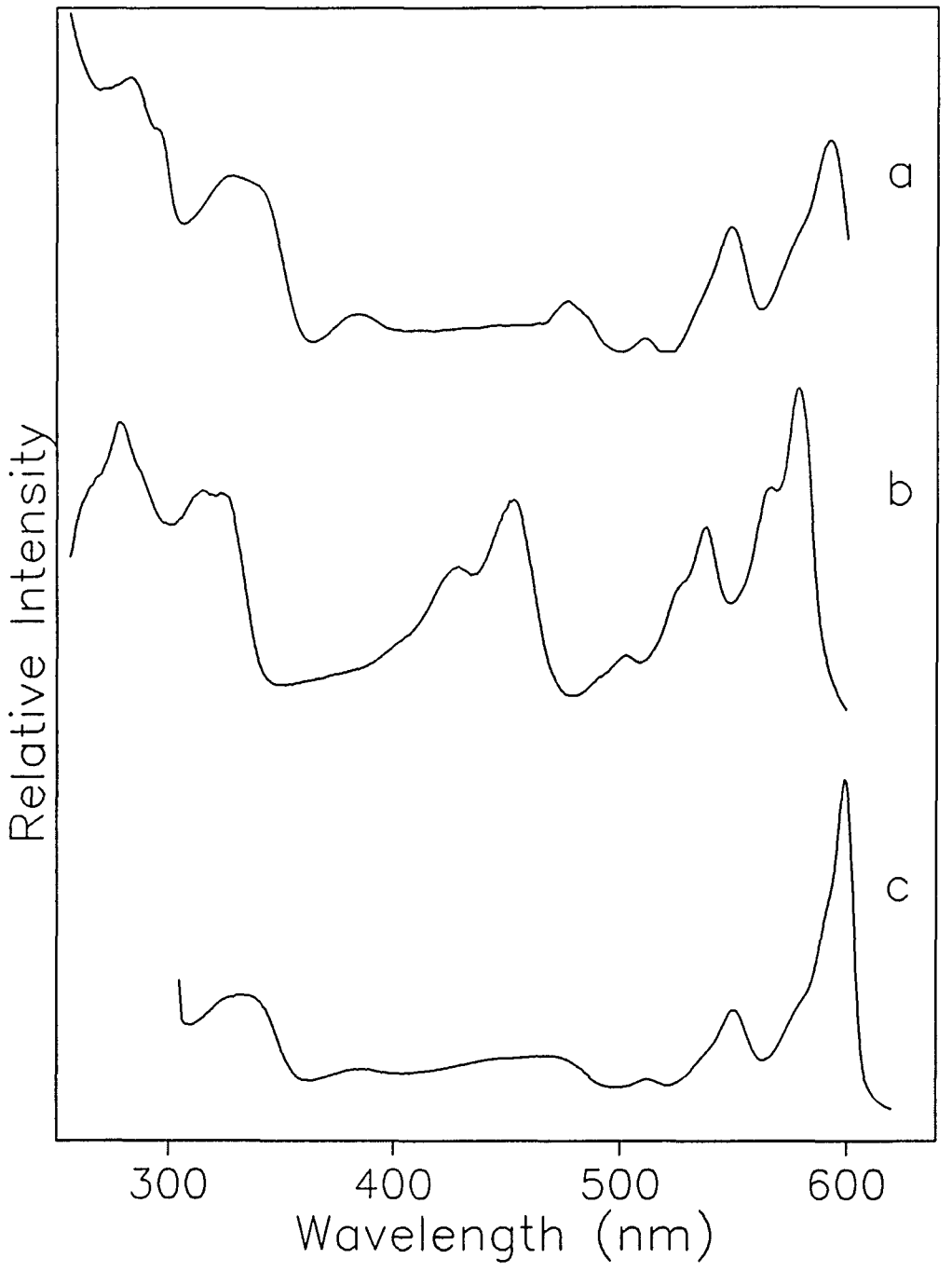

Figure 6. Fluorescence excitation spectra of hypericin. Concentrations are the same as for Figure 2. The fluorescence emission maximum was used as the excitation wavelength. Other experimental conditions same as Figure 4.

resonance Raman spectra obtained from a solid film of hypericin.[31]

Spectra were obtained for hypericin adsorbed on a silver surface from an ethanol solution,from an alkaline ethanol (pH = 12) solution and from an acidic ethanol (pH = 1) solution. The absorption spectra of these solutions are presented in Figure 7. In basic solutions, hypericin loses the proton at position 3.[25] This loss causes a change in structure along the S_1 transition dipole which can be probed with 568 nm radiation. Excitation at 568 nm is in resonance with the S_1 transition for all three hypericin solutions. In acidic solutions, there may be some perturbation of hypericin at the carbonyls, which can be probed by exciting into the S_2 transition with 458 nm laser light. The S_2 transition can be probed resonantly with 458 nm excitation for all three solutions of hypericin. The SERRS spectra for both 568 nm and 458 nm are shown in Figures 8-11 and major band positions are presented in Table III.

Overall the 458 nm excitation spectra for the neutral and basic hypericin (Figures 8 and 9) are very similar with respect to peak positions. However a few band shifts and some relative intensity differences are observed. Also, the overall intensity of the basic hypericin spectra are two to three times more intense than that for neutral hypericin. This is likely due to the increase in absorption at this wavelength. The band shifts in the basic hypericin spectra include the following: 1593 cm^{-1} (shifted from 1600 cm^{-1} of the neutral hypericin), 1366 cm^{-1} (from 1377 cm^{-1}) and 487 cm^{-1} (from 479 cm^{-1}). The relative intensity changes include increases in the bands at 1485 cm^{-1}, 1309 cm^{-1}, and 918 cm^{-1}, and a decrease in the band at 487 cm^{-1}.

The overall intensity of the 458 nm acidic spectra are comparable to those of

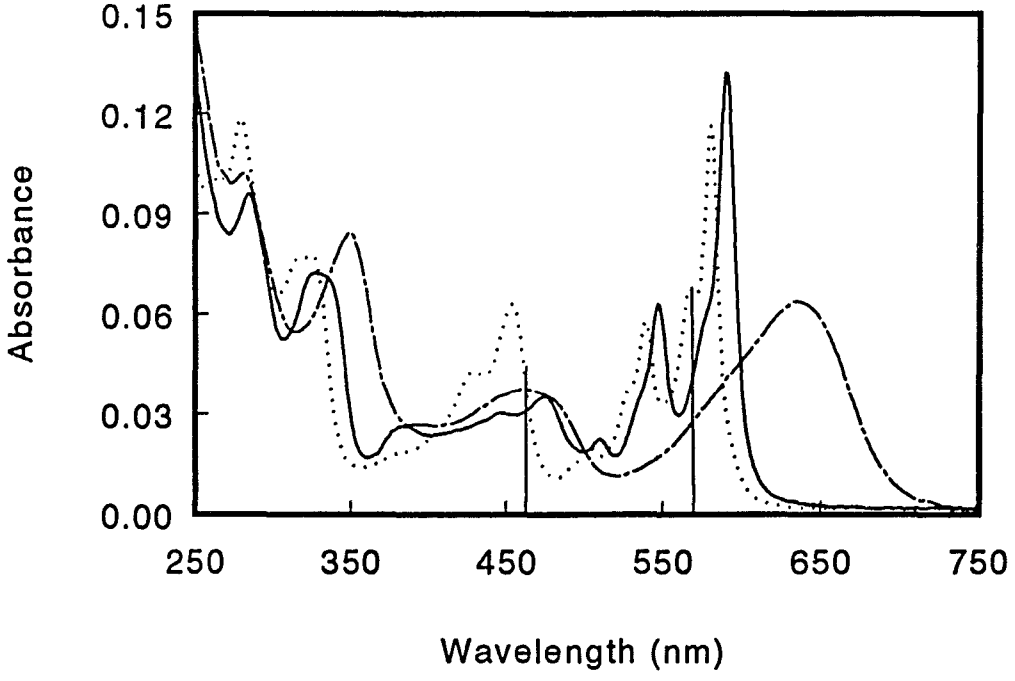

Figure 7. Absorption spectra of hypericin in ethanol solutions. Concentration was 3.8×10^{-6} M. (———) neutral ethanol, (·····) acidic ethanol pH = 1, (— · —) alkaline ethanol pH = 12. Vertical lines show Raman excitation lines.

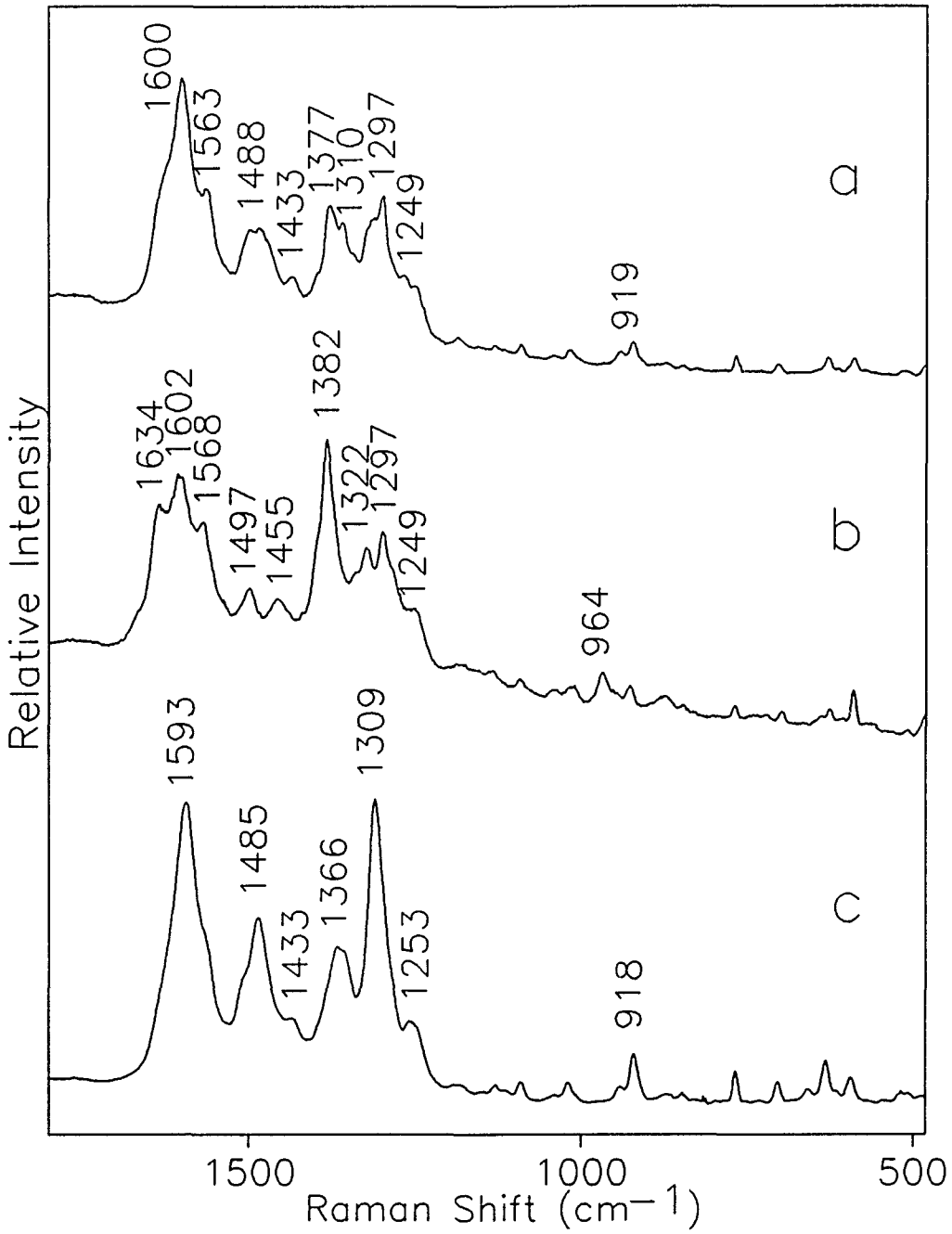

Figure 8. High frequency SERRS spectra of hypericin obtained with 458 nm excitation. Hypericin adsorbed from a) neutral ethanol solution, b) acidic solution pH = 1, c) basic solution pH =12. Integration time = 200 s, laser power was 10 mW at the sample, 77 K.

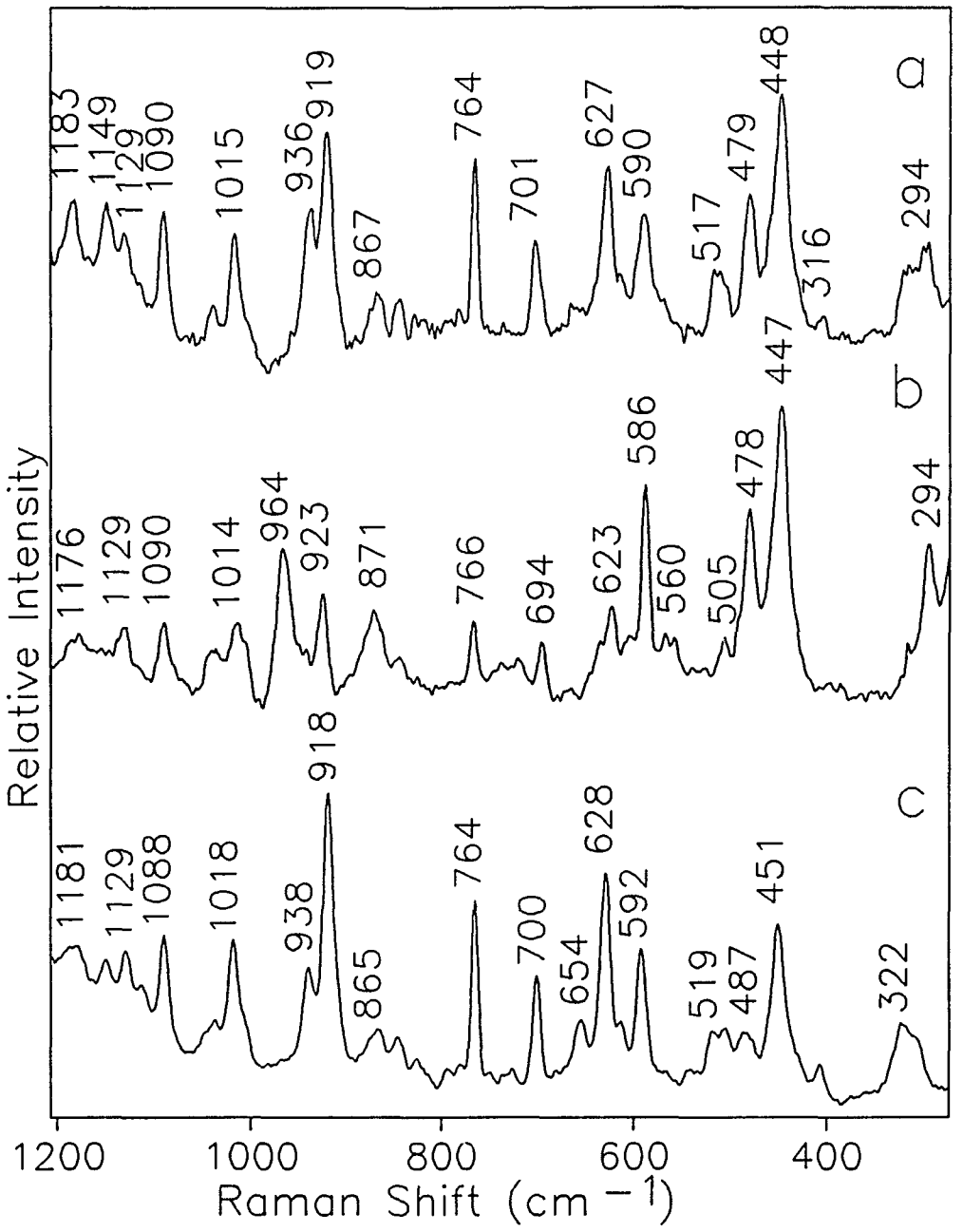

Figure 9. Low frequency SERRS spectra of hypericin obtained with 458 nm excitation. Hypericin adsorbed from a) neutral ethanol solution, b) acidic solution pH = 1, c) basic solution pH =12. Experimental conditions same as Fig. 8.

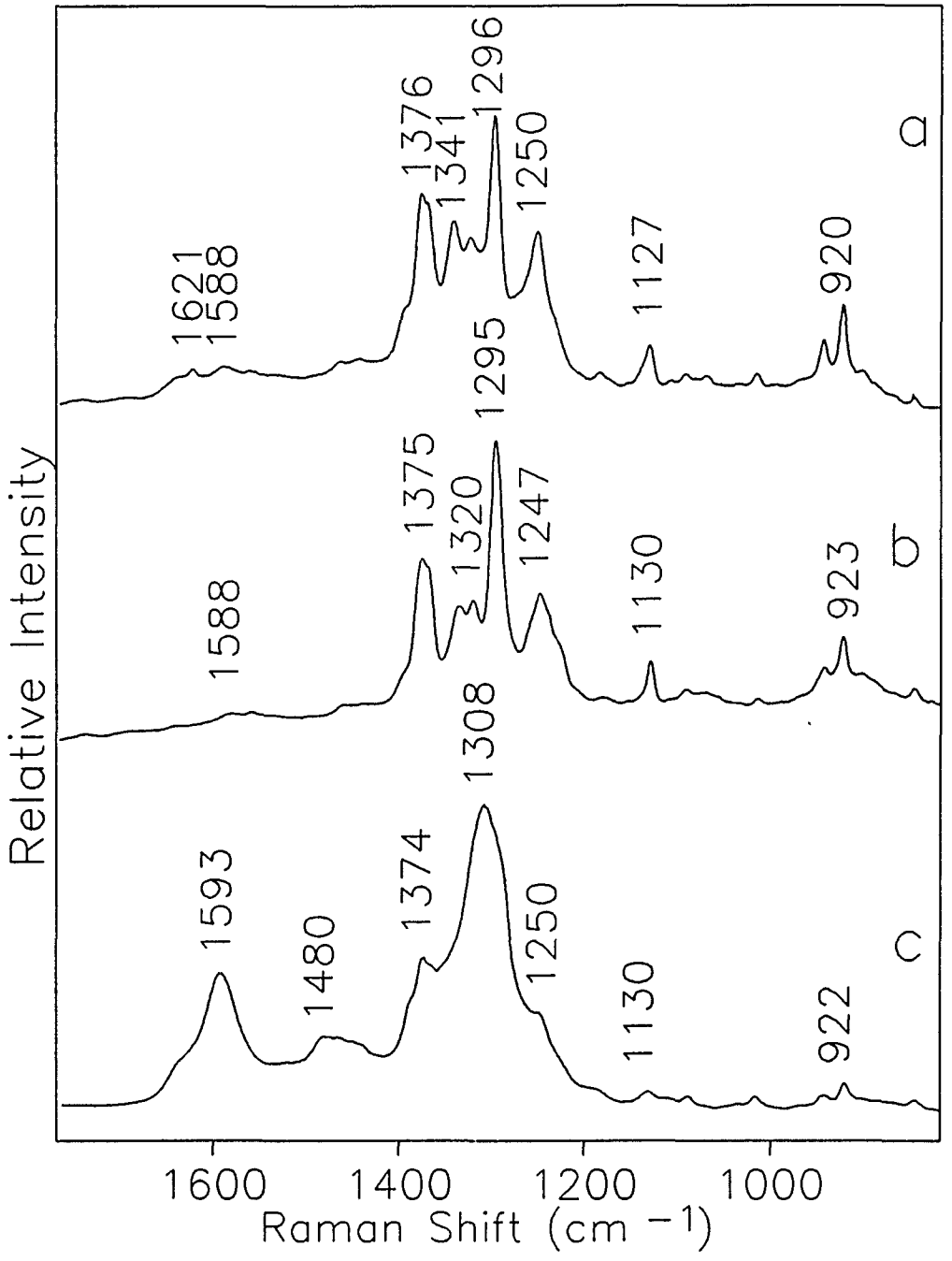

Figure 10. High frequency SERRS spectra of hypericin obtained with 568 nm excitation. Hypericin adsorbed from a) neutral ethanol solution, b) acidic solution pH = 1, c) basic solution pH =12. Integration time = 60 s, laser power 10 mW, 77 K.

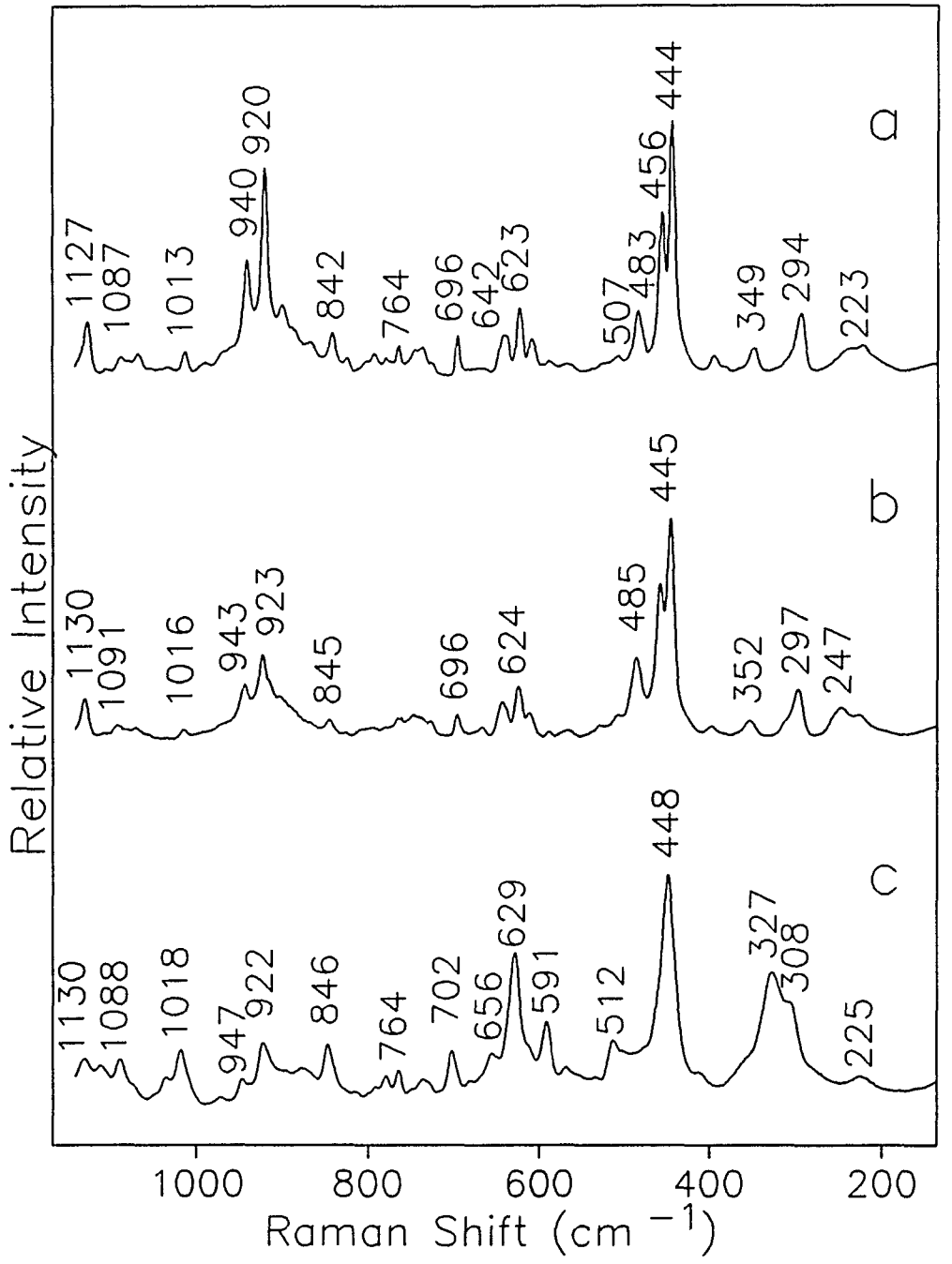

Figure 11. Low frequency SERRS spectra of hypericin obtained with 568 nm excitation. Hypericin adsorbed from a) neutral ethanol solution, b) acidic solution pH = 1, c) basic solution pH =12. Experimental conditions same as Fig. 8.

TABLE 3: SERRS spectra peak maxima (cm^{-1})

568 nm			458 nm		
hypericin	hyp + H^+	hyp + OH^-	hypericin	hyp + H^+	hyp + OH^-
1621	1621			1634	
1588	1588	1593	1600	1602	1593
			1563	1568	
		1480	1488	1497	1485
			1433	1455	1433
1376	1375	1374	1377	1382	1366
1341	1335				
1323	1320			1322	
		1308	1310		1309
1296	1295		1297	1297	
1250	1247	1250	1249	1249	1253
			1183	1176	1181
			1149		1150
1127	1130	1130	1129	1129	1129
1087	1091	1088	1090	1090	1088
1013	1016	1018	1015	1014	1018
				964	
940	943	947	936	940	938
920	923	922	919	923	918
842	845	846	867	871	865
764	764	764	764	766	764
696	696	702	701	694	700
642	643	656			654
623	624	629	627	623	628
610	612		590	586	592
		591		560	
			517		519
507	507	512		505	505
483	485		479	478	487
456	457				
444	445	448	448	447	451
349	352				
		327	316		322
294	297	308	294	294	
240	247				
223	225	225			

neutral hypericin, but there are many relative intensity differences and several large band shifts. In the high frequency region, many of the bands are shifted from 5 to 22 cm^{-1}. The relative intensity of the 1382 cm^{-1} band in the acidic hypericin spectrum is greater than that of the neutral hypericin, and changes are observed in the relative intensity of the bands in the region between 1435 cm^{-1} and 1500 cm^{-1}. In the low frequency region, most of the changes are relative intensity changes, most notably in the bands at 871 cm^{-1}, 766 cm^{-1}, 623 cm^{-1}, and 586 cm^{-1}. New bands also appear at 964 cm^{-1} and 560 cm^{-1}.

The SERRS spectra for hypericin and acidic hypericin at 568 nm are almost identical (Figures 10 and 11). This is reasonable since the absorption spectrum is very similar for both. One change that is observed with acidification is a decrease in the relative intensity of the 943 cm^{-1} and the 923 cm^{-1} bands. The basic spectrum at 568 nm is noticeably different from that of neutral hypericin. In the high frequency region, the bands at 1593 cm^{-1} and 1480 cm^{-1} are much more intense in the basic spectrum. Also, several changes are observed in the region between 1400 cm^{-1} and 1250 cm^{-1}. The band at 1308 cm^{-1} grows in dramatically and is quite broad. The neutral hypericin bands at 1296 cm^{-1}, 1323 cm^{-1} and 1341 cm^{-1} are probably masked by the broad peak at 1308 cm^{-1}.

The low frequency region also exhibits several changes in the basic spectrum. Band shifts include 947 cm^{-1} (shifted from 940 cm^{-1} of the neutral hypericin), 656 cm^{-1} (shifted from 642 cm^{-1}), 629 cm^{-1} (from 623 cm^{-1}) and 308 cm^{-1} (from 294 cm^{-1}). Relative intensity changes are also seen throughout the low frequency region. Some of the bands affected include 1018 cm^{-1}, 922 cm^{-1}, 846 cm^{-1}, 629 cm^{-1} and 512 cm^{-1}. Also new bands appear at 591 cm^{-1} and 327 cm^{-1} and the shoulders on the 448 cm^{-1} peak have disappeared.

Discussion

The absorption and fluorescence data will be discussed first followed by a discussion of the Raman data. The Type I absorption spectra are characteristic of the monomeric hypericin spectra reported by Yamazaki *et al.*[26] Over the concentration range studied, no changes in the absorption spectra were observed. The changes in the fluorescence emission spectra can readily be explained by considering the vibrational structure of the lowest electronic energy transition and a self-quenching mechanism.

The Type II spectra are similar to the spectrum of the hypericin 1,6-dioxo tautomer reported by Etzlstorfer *et al.*[38] The authors report the spectrum for the 1,6 tautomer in ethanol. The band intensities and peak positions reported are identical with those obtained for hypericin in acidic ethanol. However, it should be noted that the previous authors used a much longer reaction time to accomplish the acid catalyzed tautomerization. They also reported that it took two days of heating at 80°C for the tautomer to convert back to the hypericin isomer. In our experiments, when hypericin in acidic ethanol is neutralized with base, the absorption spectrum immediately changes back to a neutral hypericin Type I ethanol spectrum. This coupled with the fact that similar spectra are observed for all the Type II solvents, make it unlikely that a tautomer is formed under these conditions. However, it is recognized that absorption spectra are not absolute proof of structure. The Type II spectra may be indicative of protonated hypericin. Falk *et al.*[25] report the 650 nm absorption band of hypericin in concentrated sulfuric acid as being indicative of protonated hypericin. The Type II spectra are all considerably blue shifted from this value. However, it is possible that the very red 650

nm absorption band is simply a solvent effect specific for sulfuric acid and that the large increase in the S_2 band intensity observed for all Type II and aqueous sulfuric acid solutions may be a more uniform indicator of a protonated hypericin species. In concentrated sulfuric acid, the hypericin may be a doubly-protonated species as suggested by Gai *et al.*[39]. Another explanation is that the hypericin may undergo a reversible sulfonation reaction where one of the hydrogens on the rings is replaced by a SO_3^- group. Either of these reactions may be responsible for the large red shift of the absorption band. This red shift of the visible bands is reversible. When the concentrated sulfuric acid solution is diluted with ethanol the hypericin S_1 band shifts back to the blue with its absorption maximum at 581 nm. This system still exhibits the increased intensity of the S_2 band.

It is well known that hypericin forms aggregates in water. Since the spectra of hypericin in hexane, cyclohexane, toluene, chloroform, and carbon tetrachloride are very similar to the spectrum of hypericin in water, it can be assumed that it also forms aggregates in these solvents. The changes observed in the absorption spectra including the large reduction in extinction coefficients, the band broadening, the shifts in band positions and the changes in intensities are all indicators of aggregation. Aggregated species often do not fluoresce. The fluorescence obtained for all of the Type III solutions was very weak and resembled the fluorescence obtained for hypericin in ethanol. Since all of the Type III solutions contained some ethanol, the weak fluorescence is likely due to the presence of small amounts of monomeric hypericin.

An oligomeric lattice structure for hypericin aggregates in water has been

proposed by Yamazaki *et al.*[26] They propose that hypericin hydrogen bonds to other hypericin molecules through the carbonyl and the phenolic hydroxyl groups. In addition, hypericin may hydrogen bond to water molecules. Although the non-polar Type III solvents do not participate in hydrogen bonding, the similarity to the aqueous system suggests that a similar lattice structure is also present for hypericin aggregates in these solvents. This intermolecular hydrogen bonded system is not affected much by solvent. In the case of monomeric hypericin, the self-aggregates are dissociated by the solvent.

An attempt was made to correlate the solvent dependent wavelength shifts of the monomeric solutions with Taft's solvatochromatic parameters π^*, α, and β.[40,41] The π^* scale is an index of a solvent's dipolarity/polarizability. It is related to dielectric effect, and measures the ability of a solvent to stabilize a charge or dipole moment. The α parameter is a measure of a solvent's ability to donate a proton to the solute to form a hydrogen bond. The β parameter measures the ability of a solvent to accept a proton (or to donate a electron pair) in a solute to solvent hydrogen bond. The energy of the most intense absorption peak of the S_1 transition (v=0) was plotted versus each of these parameters (see Figure 12). Similar plots were also prepared for the S_2 transitions (not shown). None of these parameters were found to correlate with wavelength shift for either transition. However, if the solvents are divided into two categories, protic and aprotic, general trends can be found.

For the protic solvents, the best correlation was found to exist for α for both transitions. Thus, for protic solvents, the ability of the solvent to donate a proton to a solvent-hypericin hydrogen bond is important. The greater the hydrogen bonding donor

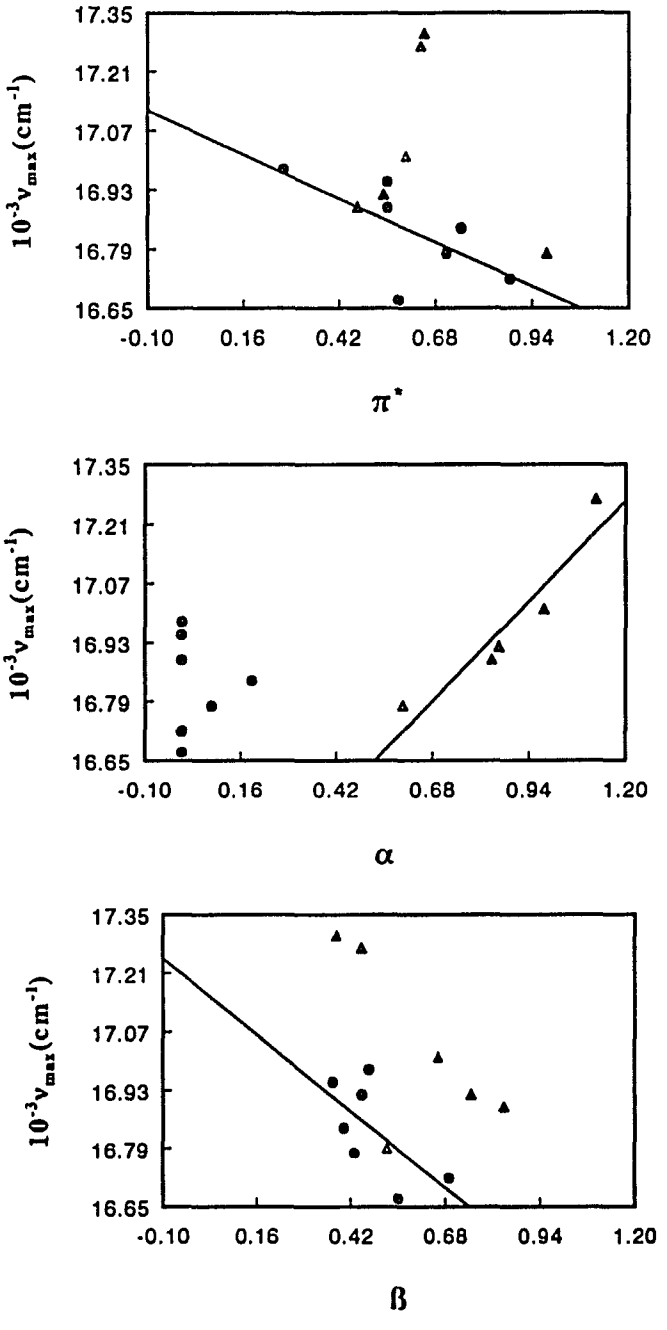

Figure 12. Plots of energy of the redmost hypericin absorption band versus Taft's solvatochromatic parameters of various solvents. ▲ protic solvents, ● aprotic solvents.

ability of the solvent, the bluer the shift in the visible absorption band. This indicates that the ground state of hypericin is stabilized by hydrogen bonding with the solvent. This effect has previously been observed for mitoxantrone (a substituted anthraquinone).[42,43] For mitoxantrone the solvent's hydrogen bonding interactions do not occur through the phenolic hydrogens, but are localized through the carbonyl groups.[42] However, this does not seem to be the case for hypericin since both transitions exhibit similar solvatochromatic behavior. Since the S_1 transition does not contain the carbonyl groups, the hydrogen bonding must involve the side hydroxy groups at positions 3 and 4. It is not known if the hydrogen bonding along the S_2 transition involves the carbonyls or the hydroxyl groups or both.

For aprotic solvents, the correlations are not as linear as for the protic solvent α plots, however general trends for both β and π^* do exist. For both the S_1 and the S_2 transitions, the absorption bands shift red as β and π^* increase. For both parameters, the linearity is slightly better for the S_2 transition (not shown). Yamazaki *et al.*[26] correlated solvent dependent wavelength shifts with both the π^* and α parameters, but found no correlation with β. For the aprotic solvents, the greater the hydrogen bond acceptor ability of the solvent or the greater the polarizability of the solvent, the greater the red shift in the peak position. This is typical behavior for a π to π^* transition, where the excited state species is stabilized by the solvent. In this case, the stabilization can occur through either solvent-solute hydrogen bonding or through the solvent's dipolarity/polarizability. Since the aprotic solvents do not contain a hydrogen atom capable of participating in a solvent-solute hydrogen bond at the carbonyl groups, these

solvents must form hydrogen bonds with the phenolic hydrogen groups at positions 1, 6, 8 and 13 or with the side hydroxy groups at positions 3 and 4 of hypericin.

Two factors that must be considered in conjunction with the analysis of SERRS spectra are the changes in resonance conditions from absorption spectral changes, and the adsorption interaction of the hypericin at the silver surface. Both 568 nm and 458 nm are in resonance for all three solutions of hypericin so there should be little differences due to resonance effects. However, the differences in the extinction coefficients at these wavelengths can cause overall intensity differences in the Raman spectra. The orientation effects are more difficult to discern, but consideration of the carbonyl band does provide some information.

The carbonyl band for *p*-quinones is normally present between 1660 cm^{-1} and 1700 cm^{-1}. For diphenoquinone the carbonyl bands are found at 1634 cm^{-1} and for hydroxyl substituted anthraquinones where intramolecular hydrogen bonding is present, the carbonyl band can shift to lower frequencies by 40 cm^{-1}.[44] The carbonyl band of hypericin has been observed in the IR at 1590 cm^{-1}.[9] This value is quite reasonable for an intramolecular hydrogen bonded system. The NMR spectrum of hypericin also indicates intramolecular hydrogen bonding between the carbonyl and the hydroxyl groups[9]. Generally, the carbonyl band is weaker in the Raman than in the IR. This coupled with the broad C-C ring stretching vibrations observed around 1600 cm^{-1} in the hypericin Raman spectra, make it difficult to determine the extent to which carbonyl bands contribute in this region. However, more information can be obtained by comparing the hypericin 458 nm and 568 nm spectra. The largest difference between the

two spectra is that the overall intensities of bands near 1600 cm^{-1} are very strong for 458 nm compared to 568 nm. The S_1 (568 nm) transition does not involve the carbonyls and therefore this vibration is not observed in the SERRS spectra. On the other hand, the carbonyl vibrations should be observed for the S_2 transition as long as the hypericin is not adsorbed parallel to the surface. The large intensity of the 1600 cm^{-1} band suggests that there is a significant carbonyl contribution to this band. The fact that all three 458 nm spectra in the 1600 cm^{-1} region are alike, coupled with their similar structures, suggests comparable orientations for all three forms of hypericin.

When the different hypericin samples were excited with 568 nm radiation, the spectra of hypericin and acidic hypericin were nearly identical, while many differences were observed for the basic hypericin spectra. These changes are caused by the removal of the proton on the hydroxyl group at position 3, which lies along the short axis of the hypericin skeleton. The two most noticeable changes in the 568 nm excited basic hypericin spectra, are the appearance of the 1593 cm^{-1} band and the intense broad band at 1308 cm^{-1}. Both of these changes can be attributed to the formation of a hydrogen bonded ring structure between the hydroxyl group at position 4 and the O^- at position 3. In fact this type of ring structure has recently been identified in a single crystal of hypericin recrystallized from pyridine.[45] For this type of structure, the 1593 cm^{-1} band is due to a ring stretch, while the 1308 cm^{-1} band is probably a combination of a C-O stretch and an in-plane OH deformation. A phenolic C-O stretch is typically found around 1250 cm^{-1},[46] while OH deformations occur between 1300 cm^{-1} and 1500 cm^{-1}.[47] These spectra support the assignment of the S_1 electronic transition as polarized along the

short axis. The hypericin and acidic hypericin, likely a protonated species, would have no structural differences along this axis and therefore the Raman spectra would be expected to be quite similar.

In the case of the 458 nm excitation spectra, the opposite spectral changes are expected. Here the spectra of the neutral hypericin and the basic hypericin are quite similar. There are some relative intensity changes, but these may result from slightly different orientations of the molecule at the surface, or the presence of OH^- may perturb the intramolecular hydrogen bonding at the carbonyls. However, much greater changes are observed for the protonated hypericin species. Again, this would be expected if the S_2 transition is polarized through the carbonyl groups where protonation occurs. The addition of H^+ may break the intramolecular hydrogen bonding and shift the carbonyl band to 1634 cm^{-1}. This is a reasonable frequency for $C{=}O^{\cdots}H^+$.

Conclusions

Hypericin was found to be monomeric in most polar organic solvents. In aqueous and non-polar solvents hypericin forms aggregates which are stabilized by intermolecular hydrogen bonding. In acidic solvents, the S_2 absorption band is very distinctive and may be indicative of protonation of the carbonyls. The solvatochromatic behavior of hypericin is dependent upon the nature of the solvent. For protic solvents, the hydrogen bond donor ability of the solvent is important for stabilizing the ground state of hypericin. On the other hand, aprotic solvents interact by stabilizing the excited state species through their polarizability and their hydrogen bond acceptor abilities.

The Raman data support the previous polarization assignments for the electronic transitions. The lowest energy transition (ca. 590 nm) has been assigned to the π-π^* transition polarized along the short axis of the hypericin skeleton, while the S_2 transition (ca. 475 nm) is a π-π^* transition polarized through the carbonyl axis of the hypericin. The presence of the carbonyl band at 1600 cm^{-1} in the 458 nm spectra and its absence in the 568 nm spectra support these assignments. These assignments are also corroborated by the spectra obtained for the protonated and deprotonated hypericin species. The removal of the proton on the hydroxyl group at position 3 results in a structure that is different from hypericin along the short axis of the molecule, but is identical in structure through the carbonyl axis. This is reflected in the SERRS spectra. As expected, excitation into the S_2 transition with 458 nm radiation results in nearly identical spectra for hypericin and deprotonated hypericin. On the other hand, excitation into the S_1 transition with 568 nm radiation results in spectral differences indicative of the change in structure along this transition axis. The opposite is true for the protonated hypericin species. The structural perturbation is along the carbonyl axis and the structure along the short axis is the same as neutral hypericin. In this case, the 568 nm spectra of hypericin and protonated hypericin are similar, whereas the 458 nm acidic hypericin spectra have many differences from the neutral hypericin spectra.

Acknowledgements

The authors wish to thank Dr. Jacob Petrich and his students for the use of the fluorimeter. This work was supported by a grant from the National Institute of Health (GM35108 TMC).

References

(1) Pace, N.; Mackinney, G. *J. Am. Chem. Soc.* **1941,** *63,* 2570.

(2) Giese, A. C. In *Photophysiology Current Topics in Photobiology and Photochemistry,* Vol VI, Giese, A.C., Ed.; Academic Press: New York, 1971; 77.

(3) Knox, J. P.; Dodge, A. D. *Plant Cell Environ.* **1985,** *8,* 19.

(4) Durán, N.; Song, P.-S. *Photochem. Photobiol.* **1986,** *43,* 677.

(5) Brockmann, H. H. *Progress in Organic Chemistry,* Vol 1, Cook, J. W., Ed.; Academic Press: New York, 1952; 64.

(6) Pace, N. *Am. J. Physiol.* **1942,** *136,* 650.

(7) Giese, A. C. In *Photochemical and Photobiological Reviews,* Vol 5, Smith, K. C., Ed.; Plenum Press: New York, 1980; 229.

(8) Walker, E. B.; Lee, T. Y.; Song, P.-S. *Biochim. Biophys. Acta* **1979,** *587,* 129.

(9) Tao, N.; Orlando, M.; Hyon, J.-S.; Gross, M.; Song, P.-S. *J. Am. Chem. Soc.* **1993,** *115,* 2526.

(10) Meruelo, D.; Lavie, G.; Lavie, D. *Proc. Natl. Acad. Sci. USA* **1988,** *85,* 5230.

(11) Lavie, G.; Valentine, F.; Levin, B.; Mazur, Y.; Gallo, G.; Lavie, D.; Weiner, D.; Meruelo, D. *Proc. Natl. Acad. Sci. USA* **1989,** *86,* 5963.

(12) Carpenter, S.; Kraus, G. A. *Photochem. Photobiol.* **1991,** *53,* 169.

(13) Hudson, J. B.; Lopez-Bazzocchi, I.; Towers, G. H. N. *Antivir. Res.* **1991,** *15,* 101.

(14) Lopez-Bazzocchi, I.; Hudson, J. B.; Towers, G. H. N. *Photochem. Photobiol.* **1991,** *54,* 95.

(15) Degar, S.; Prince, A. M.; Pascual, D.; Lavie, G.; Levin, B.; Mazur, Y.; Lavie, D.; Ehrlich, L. S.; Carter, C.; Meruelo, D. *Aids Res. Hum. Retroviruses* **1992,** *8,* 1929.

(16) Heitz, J. R. In *Light Activated Pesticides,* Heitz, J. R.; Downum, K. R., Eds.; American Chemical Society: Washington D.C., 1987; 38.

(17) Knox, J. P.; Samuels, R. I.; Dodge, A. D. In *Light Activated Pesticides,* Heitz J. R.; Downum, K. R., Eds.; American Chemical Society: Washington DC, 1987; 265.

(18) Yang, K.-C.; Prusti, R. K.; Walker, E. B.; Song, P.-S.; Watanabe, M.; Furuya, M. *Photochem. Photobiol.* **1986,** *43,* 305.

(19) Jardon, P.; Lazortchak, N.; Gautron, R. *J. Chim. Phys. Phys-Chim. Biol.* **1987,** *84,* 1141.

(20) Thomas, C.; MacGill, R. S.; Miller, G. C.; Pardini, R. S. *Photochem. Photobiol.* **1992,** *55,* 47.

(21) Weiner, L.; Mazur, Y. *J. Chem. Soc. Perkin Trans. 2* **1992,** 1439.

(22) Malkin, J.; Mazur, Y. *Photochem. Photobiol.* **1993,** *57,* 929.

(23) Song, P.-S.; Häder, D.-P.; Poff, K. L. *Photochem. Photobiol.* **1980,** *32,* 781.

(24) Song, P.-S.; Kim, I.-H.; Florell, S.; Tamai, N.; Yamazaki, T.; Yamazaki, I. *Biochim. Biophys. Acta* **1990,** *1040,* 58.

(25) Falk, H.; Meyer, J.; Oberreiter, M. *Monatsh. Chem.* **1992,** *123,* 277.

(26) Yamazaki, T.; Nobuhiro, O.; Yamazaki, I.; Song, P.-S. *J. Phys. Chem.* **1993,** *97,* 7870.

(27) Pace, N. *J. Am. Chem. Soc.* **1939,** *61,* 3594.

(28) Scheibe, G.; Schöntag, A. *Chem. Ber.* **1942,** *75,* 2019.

(29) Brockmann, H.; Kluge, F.; Muxfeldt, H. *Chem. Ber.* **1957,** *90,* 2302.

(30) Jardon, P.; Gautron, R. *J. Chim. Phys. Phys-Chim. Biol.* **1989,** *86,* 2173.

(31) Raser, L. N.; Kolaczkowski, S. V.; Cotton, T. M. *Photochem. Photobiol.* **1992,** *56,* 157.

(32) Gill, M.; Gimenez, A.; McKenzie, R. W. *J. Nat. Prod.* **1988,** *51,* 1251.

(33) Falk, H.; Schmitzberger, W. *Monatsh. Chem.* **1992,** *123,* 731.

(34) Michaeli, A.; Regev, A.; Mazur, Y.; Feitelson, J.; Levanon, H. *J. Phys. Chem.* **1993,** *97,* 9154.

(35) Gai, F.; Fehr, M. J.; Petrich, J. W. *J. Am. Chem. Soc.* **1993,** *115,* 3384.

(36) Bonnett, R.; Berenbaum, M. In *Ciba Foundation Symposium 146 Photosensitizing Compounds: their Chemistry Biology and Clinical Use,* Bock, G.; Harnett, S., Eds.; John Wiley and Sons: Chichester, 1989; 40.

(37) Valdes-Aguilera, O.; Neckers, D. C. *Acc. Chem. Res.* **1989,** *22,* 171.

(38) Etzlstorfer, C.; Falk, H.; Oberreiter, M. *Monatsh. Chem.* **1993,** *124,* 923.

(39) Gai, F.; Fehr, M. H.; Petrich, J. W. *J. Phys. Chem.* **1994,** *98,* 5784.

(40) Kamlet, M. J.; Abboud, J. L.; Abraham, M. H.; Taft, R. W. *J. Org. Chem.* **1983,** *48,* 2877.

(41) Marcus, Y. *Chem. Soc. Revs.* **1993,** *22,* 409.

(42) Lee, B. S.; Dutta, P. K. *J. Phys. Chem.* **1989,** *93,* 5665.

(43) Lin, S.; Struve, W. S. *J. Phys. Chem.* **1991,** *95,* 2251.

(44) Josien, M.-L.; Fuson, N.; Lebas, J.-M.; Gregory, T. M. *J. Chem. Phys.* **1953,** *21,* 331.

(45) Freeman, D.; Frolow, F.; Kapinus, E.; Lavie, D.; Lavie, G.; Meruelo, D.; Mazur, Y. *J. Chem. Soc., Commun.* **1994,** 891.

(46) Colthup, N. B.; Daly, L. H.; Wiberley, S. E. *Introduction to Infrared and Raman Spectroscopy,* 2nd ed.; Academic Press: New York, 1975.

(47) Nakanishi, K.; Solomon, P. H. *Infrared Absorption Spectroscopy,* 2nd ed.; Holden-Day Inc: Oakland, 1977.

CHARACTERIZATION OF THE PHOTORECEPTOR OF *STENTOR COERULEUS* BY SURFACE ENHANCED RESONANCE RAMAN SCATTERING SPECTROSCOPY

A paper submitted to *Journal of Physical Chemistry*

Jeanne L. Wynn, Jae-Ho Kim, Ningbing Tao,

Renke Dai, Pill-Soon Song, and Therese M. Cotton

Abstract

Stentorin is the photoreceptor responsible for both the step-up photophobic response and the negative phototaxis of *Stentor coeruleus*. Three protein complexes have been isolated from *Stentor*: stentorin I, stentorin II, and stentorin IIB. The structure of the chromophore for each of these complexes was investigated using surface enhanced resonance Raman scattering (SERRS) spectroscopy. The chromophore of each complex was found to be identical or very similar to that of the stentorin free chromophore. In addition, it was found that SERRS can easily distinguish stentorin from the photodynamic pigment hypericin, even though the two structures are very similar.

Abbreviations

CHAPS, (3-[(3-Cholamidopropyl)dimethylammonio]-1-propanesulfonate); DTT, dithiothreitol; EDTA, ethylenediaminetetraacetic acid; HPLC, high performance liquid chromatography; SDS, sodium dodecylsulfate; TCA, trichloroacetic acid; PAGE, polyacrylamide gel electrophoresis.

Introduction

Stentor coeruleus is a blue-green ciliate that has been shown to exhibit photosensitive behavior including both a step-up photophobic response and a negative

phototaxis.[1,2] The former response occurs when a cell encounters a sudden increase in light intensity. When a ciliate cell encounters a region of higher light intensity, it will swim away from the light source. Phototaxis occurs when an organism shows an oriented movement in response to impinging or scattered light. The negative phototaxis response of *Stentor* has been documented by observing that the organisms swim in a direction parallel to and away from the direction of light propagation. This behavior suggests that they are capable of perceiving the direction of light stimulus.

The blue-green pigment of *Stentor* is located in small vesicles which are aligned in rows just below the cell surface.[3] The absorption spectrum of this pigment was first measured in 1873 by Lankester[4], and at this time he called the pigment stentorin. Subsequently Møller[5] investigated the absorption and fluorescence properties of the pigment. The action spectra for the light avoidance behavior of *Stentor coeruleus* was obtained by Wood[6] and found to match the absorption spectrum of stentorin, indicating that stentorin is the photoreceptor responsible for the organisms photophobic response and its negative phototaxis. Two distinct forms of the stentorin pigment called stentorin I and stentorin II were isolated.[5] Stentorin I is fluorescent and ethanol soluble, whereas stentorin II is weakly fluorescent and non-extractable in ethanol. Møller's studies also concluded that both pigments belonged to the meso-naphthodianthrone group of compounds, and that they were structurally very similar to the photodynamic pigment hypericin. In fact, until recently it was believed that the chromophore of *Stentor* was hypericin. However recent studies by Tao and co-workers[7] have determined that the *Stentor* chromophore is structurally different from that of hypericin. Two possible

structures for stentorin have been proposed and these, along with the structure of hypericin, are shown in Figure 1.

Several characterization studies have been performed to elucidate the structural and functional differences between the stentorins.[3,8,9] The apparent molecular weight of stentorin I determined by SDS PAGE is 68,000 and 52,000 at 10% and 13% gels respectively. The molecular weight determined by size exclusion HPLC is 102,000. Stentorin II is a larger molecular assembly that is probably composed of several proteins. Its molecular weight is thought to be greater than 805,000.[8] Other properties that have been compared include absorption, fluorescence and circular dichroism. For stentorin I, the absorption maximum is at 610 nm and the fluorescence maximum is at 618 nm. It is highly fluorescent and does not show a strong circular dichroism signal in the visible region. In contrast, stentorin II is weakly fluorescent and has a strong circular dichroism signal. The absorption and fluorescence maxima for stentorin II are located at 620 nm and 626 nm respectively.[8] Another difference between the two stentorin pigments is that stentorin II exhibits an ultrafast primary photoprocess, whereas stentorin I does not. It is believed that stentorin II acts as the primary photoreceptor of *Stentor coeruleus*. A proton dissociation mechanism has been proposed as the primary photoprocess, however a photoinduced electron transfer is also possible.[9-11]

Recently Dai[12] isolated two subunits, stentorin IIA and stentorin IIB, from the stentorin II complex. The stentorin IIA complex is a non-chromophoric subunit, whereas the stentorin IIB subunit contains the chromophore covalently linked to a 50 kDa protein. The absorption, fluorescence and visible circular dichroism properties of the stentorin IIB

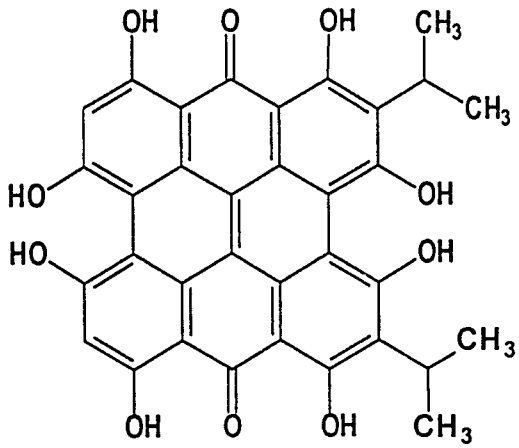

1

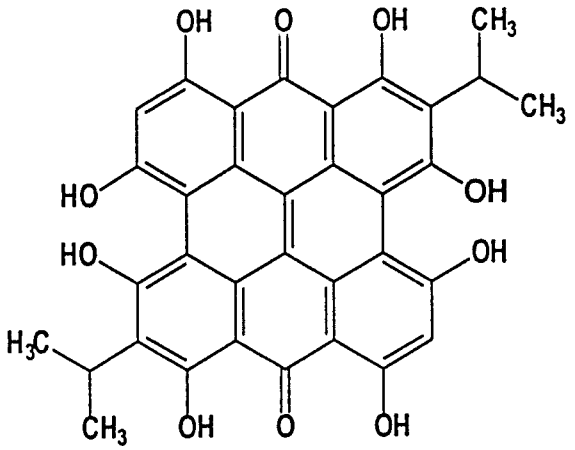

2

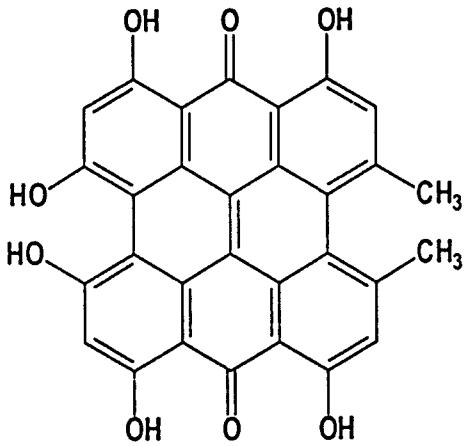

Figure 1. Possible structures 1 and 2 for the stentorin chromophore and the structure of hypericin.

complex are similar to stentorin II. Stentorin IIB is believed to retain the spectral integrity and primary photoreactivity of *Stentor coeruleus*.

In this study Raman spectroscopy is used to elucidate structural information about the chromophore of the stentorin proteins. Currently it is unknown if the chromophore of stentorin I and stentorin II is the same. Various attempts to cleave the chromophore from stentorin II and extract it, including hydrolysis with concentrated HCl, as well as with NaOH, at elevated temperatures, have been unsuccessful. However, this is not an isolated case. The native green pigment in *Aspergillus parasiticus* was reported to be a high molecular weight material that is also resistant to direct structural analysis.[13] It is our speculation that polymerization of stentorin may be responsible for the resistant nature of the stentorin II. It is known that an EC mechanism, *i.e.*, a reversible electron transfer followed by a chemical step which converts the oxidized product to some other species, often occurs during the oxidation of phenols.[14-16] "Head to tail" polymerization following oxidation of unprotected phenol was reported to result in the formation of polyphenylenoxide polymers.[16] An oxidative polymerization also occurs in hypericin.[17] Since the stentorin and hypericin are rather closely related in structure, it is possible that this type of oxidative polymerization also takes place in stentorin II thereby leading to the formation of a large complex.

The surface enhanced resonance Raman scattering (SERRS) spectra of stentorin I, stentorin II and stentorin IIB were compared to both the spectra of the free stentorin chromophore and hypericin. SERRS spectroscopy is a technique that is particularly well suited for the study of chromophores in biological molecules.[18] SERRS provides two

major advantages that make stentorin an ideal candidate for this technique. First, by exciting into an absorption band of the chromophore, the chromophore vibrational bands are observed with minimal interference from the surrounding protein matrix. Second, the intense fluorescence of the stentorin is quenched by the metal surface, allowing the Raman spectra to be readily observed.

Material and Methods

Stentorin isolation has been described elsewhere[8,12] and is summarized as follows. *Stentor* cell pellets were extracted with 20 mM Tris buffer (pH 7.8) containing 2% CHAPS, 20% sucrose, 1 mM EDTA, and 1 mM DTT. The extraction solution was centrifuged at 30,000 xg for 60 minutes and the supernatant (crude extract) was subjected to size exclusion chromatography (Bio-gel, A 1.5). Stentorin II was eluted with the void volume and stentorin I was fractionated at the fraction corresponding to around 80 kDa. Stentorin II was further purified by a hydroxylapatite column. The remaining stentorin I was eluted using 0.4% of CHAPS in Tris buffer and the stentorin II was then eluted with 0.2 M phosphate buffer (pH 7.8) containing 0.5% CHAPS, 1 mM EDTA, and 1 mM DTT. The resulting stentorin II solution was further purified by a hydrophobic benzylamine-agarose interaction column. After the non-chromophoric containing fraction (stentorin IIA) was eluted by non-detergent Tris buffer, Stentorin IIB was eluted by applying Tris buffer containing 1% CHAPS, 1% octyl-glucoside, 1 mM EDTA and 1 mM DTT.

Isolated stentorin II and IIB were precipitated by 10% TCA. Stentorin II or IIB pellets were obtained by centrifuging the TCA treated solution at 16,000 xg for 20

minutes. These pellets were then washed with doubly distilled H_2O and centrifuged under the same conditions. The pellets were then placed in a 2% SDS in 20 mM Tris buffer (pH 7.8) solution. The solutions were incubated with vibration at room temperature for two hours. The resulting solution was submitted for Raman measurements. In order to study the chromophore of these protein complexes, it is desirable for the chromophore to be adsorbed as close as possible to the SERRS surface. Therefore, the stentorin solutions were partially denatured by the addition of hydrochloric acid to bring the solution pH to 1. The isolated stentorin chromophore was prepared by sonication of the *Stentor* cells in acetone and then purified by reversed phase HPLC[7]. The purified stentorin chromophore was then placed in HPLC grade methanol. Hypericin, HPLC purified, was obtained from Carl Roth GmbH, Karlsruhe, Germany and dissolved in HPLC grade methanol.

Absorption spectra were obtained for the hypericin solution and each of the stentorin solutions using a Perkin Elmer Lambda 6 spectrophotometer. All spectra were obtained at a scan rate of 600 nm/sec and a slit width of 1 nm. The absorption spectra were collected versus the appropriate background spectrum.

The SERRS spectra were collected using a Spex Triplemate spectrometer with a Princeton Instrument CCD detector (model LN1152) cooled to -120°C. A Coherent Ar^+ 200 series laser was used for the 458 nm excitation line, and a Coherent Kr^+ 100 series laser was used for the 568 nm excitation line. The laser power at the sample was approximately 10 mW and scattered radiation was collected in a backscattered configuration. Vacuum deposited silver island films were used as the SERRS substrates.

The films were prepared by depositing 50 Å of silver on to clean glass slides at 0.2 Å/s. The slides were then immersed in the solution of interest for 5 to 15 minutes, removed from solution, rinsed with deionized water and placed in an optical dewar containing liquid nitrogen. The SERRS substrates for the hypericin and stentorin chromophore solutions were immersed for 5 minutes, and the stentorin protein solutions substrates were immersed for 15 minutes. The resulting spectra were plotted using Spectra Calc (Galactic Software) and are baseline corrected.

Results

The absorption spectra of the solutions used for this Raman study are presented in Figure 2. The spectra are all very similar with respect to peak shape, however there are differences in peak positions. Hypericin is the most blue shifted with its visible absorption maximum at 588 nm. The free stentorin chromophore peak maximum is found at 595 nm. The visible absorption maxima of the stentorin protein complexes are redshifted from this value to 610 nm and 620 nm for Stentorin I and both Stentorin II solutions respectively. In terms of peak positions, Stentorin II and IIB have identical absorption spectra. However, stentorin II has a higher protein contribution. After acid denaturation the absorption maxima were shifted for each of the stentorin protein complexes. Stentorin I was shifted to 584 nm, stentorin II to 612 nm and stentorin IIB to 608 nm. The blue shifts of the absorption maxima are evidence that some denaturation of the proteins has occurred near the chromophore for each of the stentorin complexes, although the extent is not known.

In spite of the differences in the absorption spectra, both Raman excitation lines are

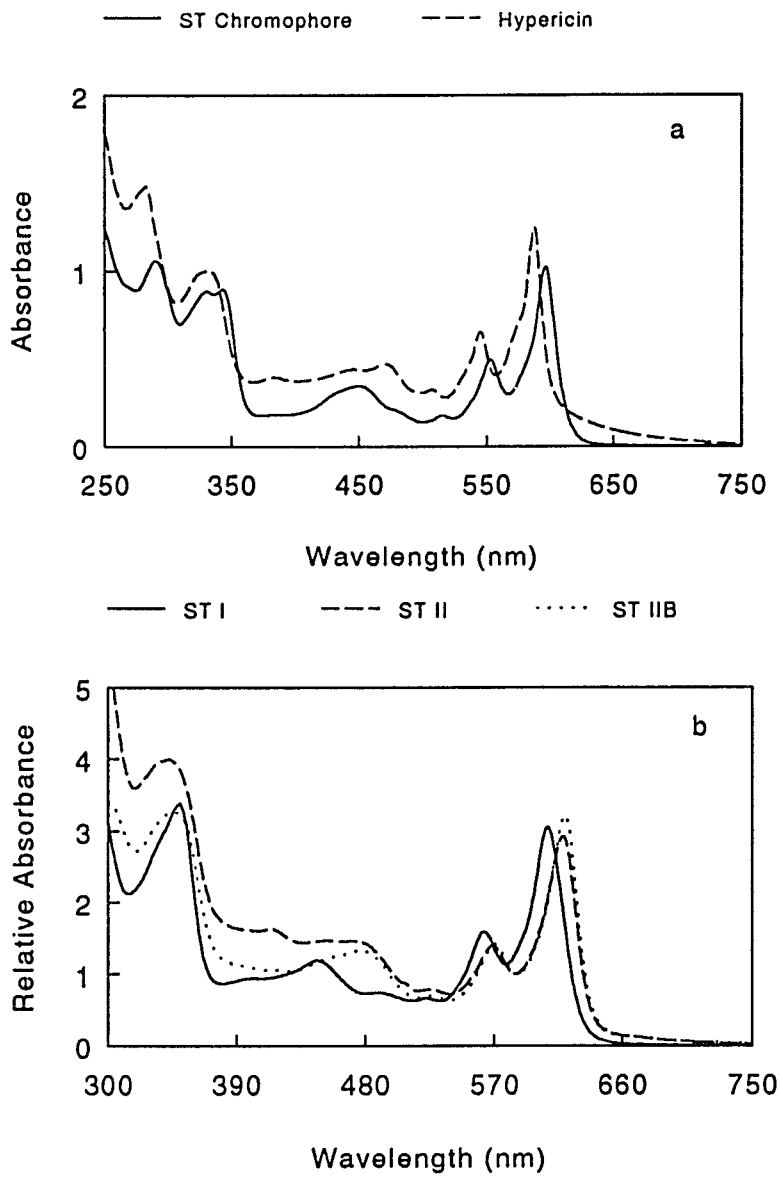

Figure 2. Absorption spectra of a) hypericin and stentorin chromophore in methanol. Concentrations were around 3 x 10^{-5} M b) stentorin protein complexes in aqueous buffer solutions. Scan rate = 600 nm/min, slit width = 1 nm, path length = 1 cm.

in resonance for all the species studied. Initially SERRS spectra were obtained for the intact protein complexes (not shown), but the spectra were overwhelmed by fluorescence and the Raman bands were not observed. Therefore, it was necessary to acid denature the proteins in order to expose the chromophore. This allowed the chromophore to adsorb close enough to the metal surface so that its fluorescence was effectively quenched. The SERRS spectra for 568 nm excitation are shown in Figures 3 and 4, and the 458 nm excitation spectra are presented in Figures 5 and 6. In addition, major band positions for all spectra appear in Table 1.

A comparison of the high frequency regions (Figs. 3 and 5) of the hypericin and the stentorin chromophore reveals that the two species have similar Raman spectra in terms of the overall appearance. This is true for both excitation wavelengths. Although many of the same bands are observed in both spectra, most of the stentorin chromophore bands between 1650 and 1250 cm^{-1} are shifted 6 to 17 cm^{-1} from those of hypericin. The notable exception is the 568 nm 1370 cm^{-1} band (1378 cm^{-1} for 458 nm). This band is located at the same frequency for both the hypericin and the free chromophore spectra. Two differences specific to the 568 nm spectra (Fig. 3) are that the hypericin bands at 942 cm^{-1} and 922 cm^{-1} are much more intense than the corresponding bands in the stentorin chromophore spectrum, and the stentorin spectrum has a greater relative contribution from the vibrations at 1640 cm^{-1} and 1550 cm^{-1}. The low frequency region (Figs. 4 and 6) of the hypericin and the stentorin chromophore also contain many of the same bands, but again most are shifted in frequency and the relative intensities are different. In addition, there are several bands that are unique to either the

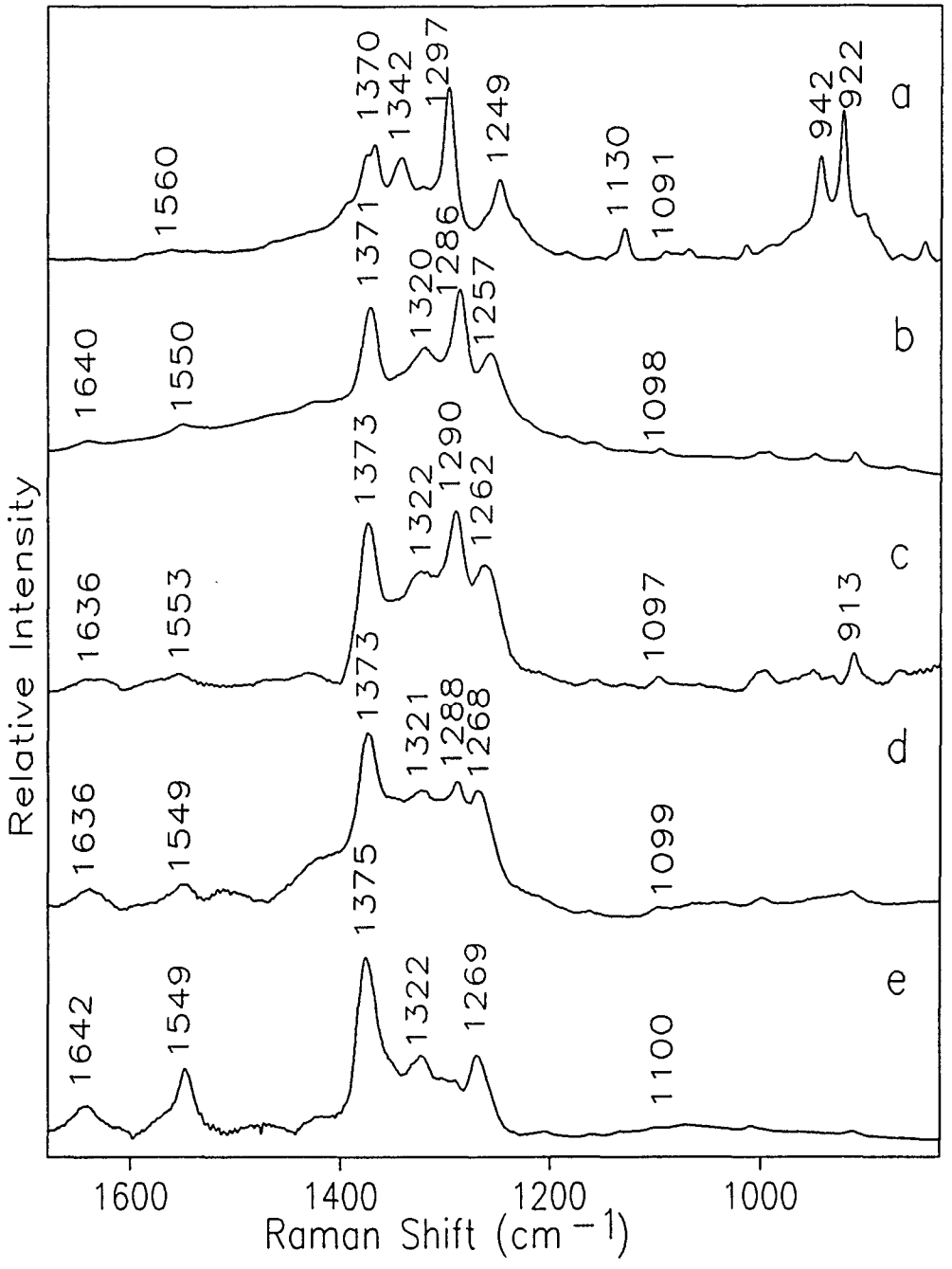

Figure 3. High frequency SERRS spectra obtained with 568 nm excitation a) hypericin, b) stentorin chromophore, c) stentorin I, d) stentorin II, e) stentorin IIB. Laser power 10 mW, 77 K, integration times: a),c),e) 60 s, b) 20 s, d) 200 s.

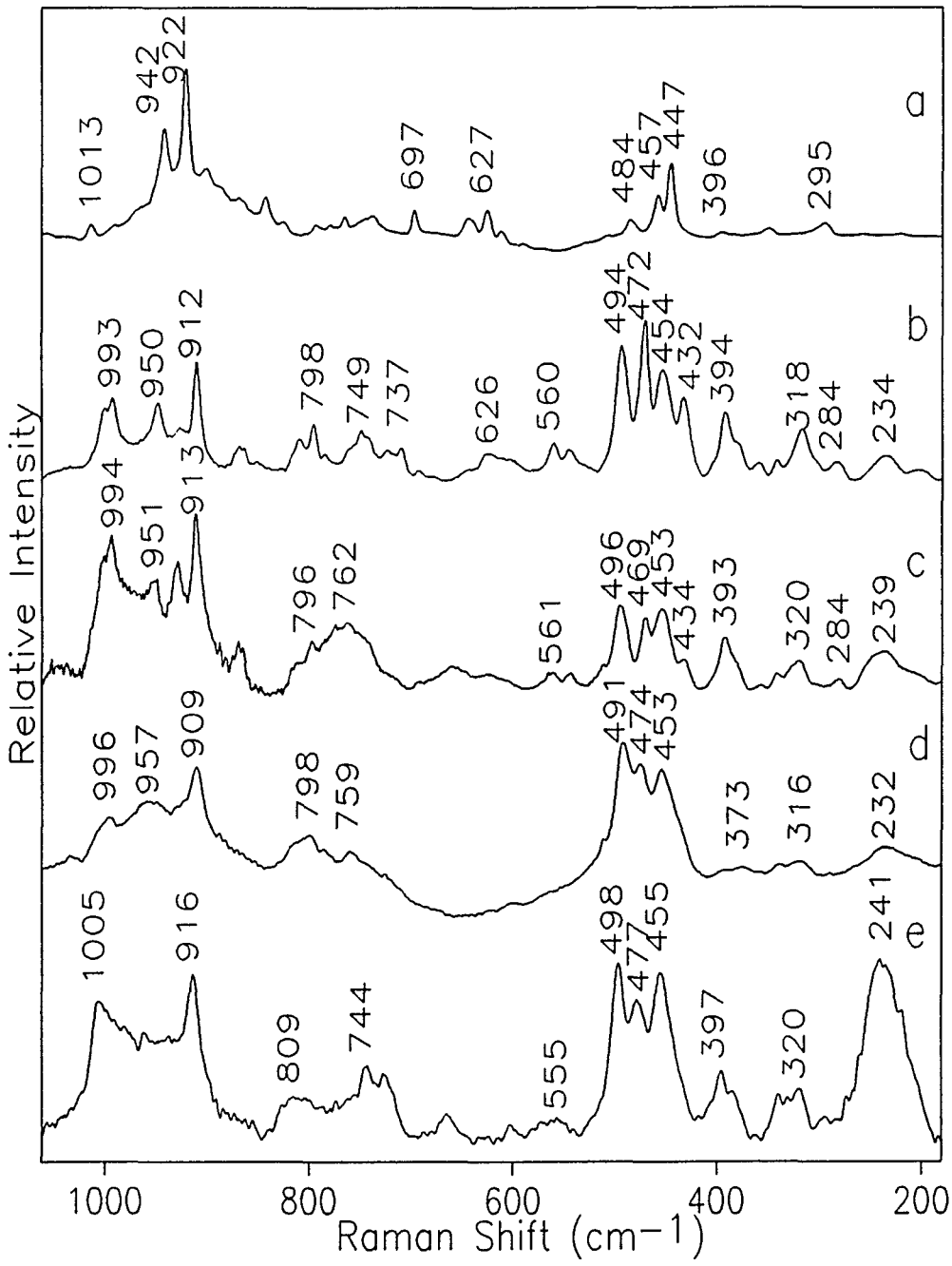

Figure 4. Low frequency SERRS spectra obtained with 568 nm excitation a) hypericin, b) stentorin chromophore, c) stentorin I, d) stentorin II, e) stentorin IIB. Laser power 10 mW, 77 K, integration times: a) 20 s, b) 60 s, c), d), e) 200 s.

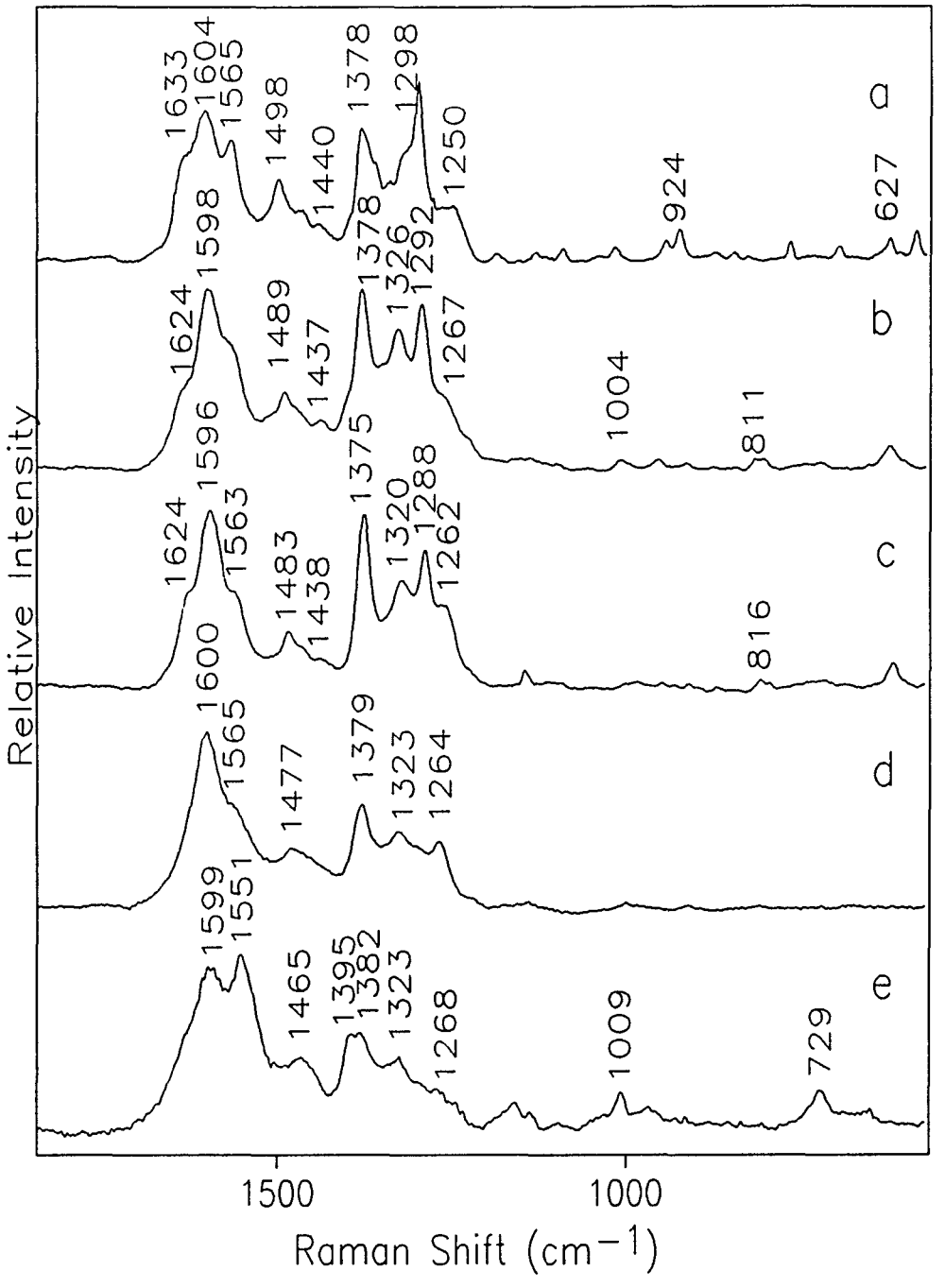

Figure 5. High frequency SERRS spectra obtained with 458 nm excitation a) hypericin, b) stentorin chromophore, c) stentorin I, d) stentorin II, e) stentorin IIB. Laser power 10 mW, 77 K, all integration times 200 s.

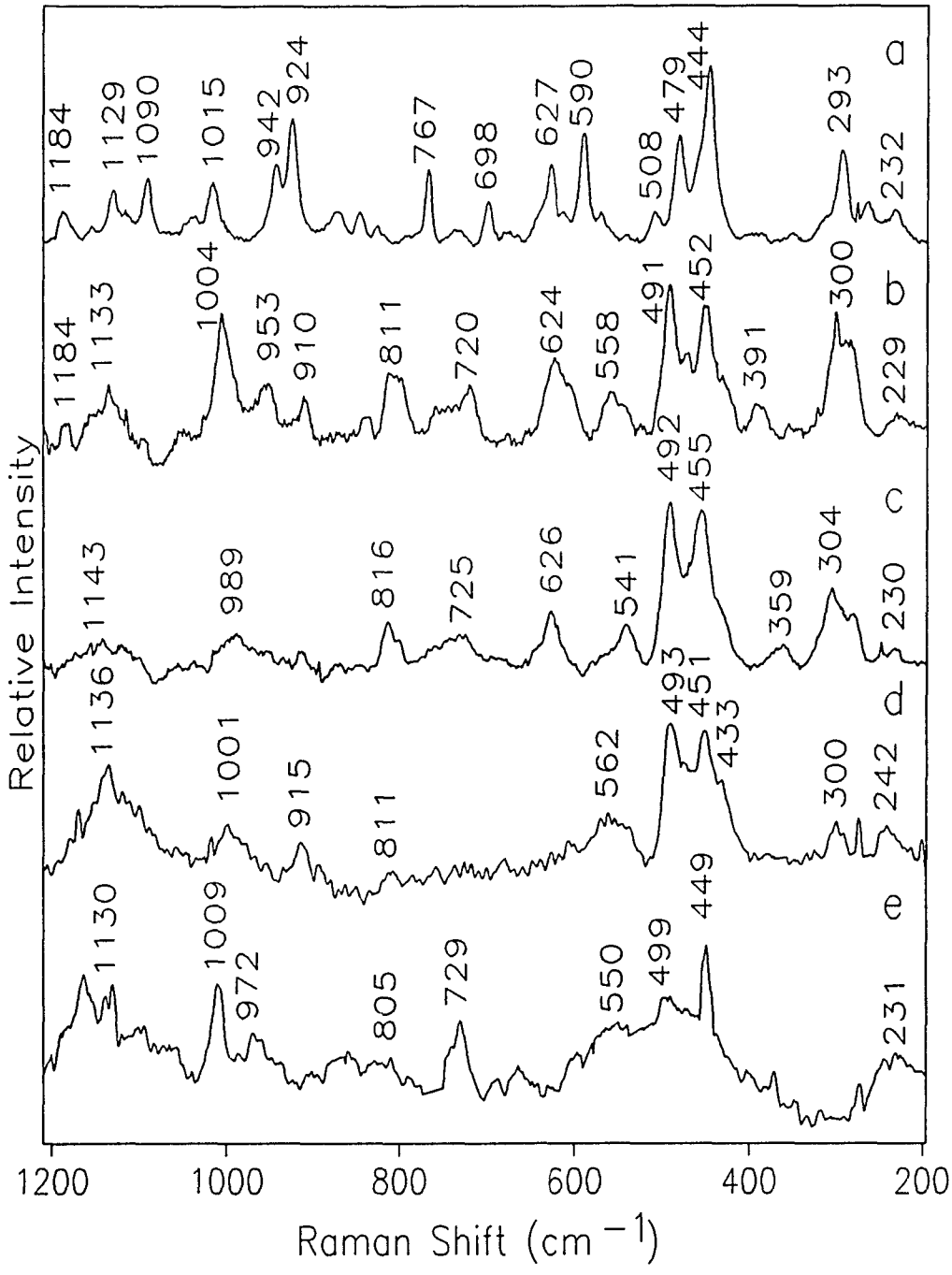

Figure 6. Low frequency SERRS spectra obtained with 458 nm excitation a) hypericin, b) stentorin chromophore, c) stentorin I, d) stentorin II, e) stentorin IIB. Experimental conditions same as Fig. 5.

TABLE 1: SERRS spectra peak maxima (cm^{-1})

		568 nm					458 nm		
Hyp	Chrom	ST I	ST II	ST IIB	Hyp	Chrom	ST I	ST II	ST IIB
	1640	1636	1636	1642	1633	1624	1624		
					1604	1598	1596	1600	1599
1560	1550	1553	1549	1549	1565		1563	1565	1551
					1498	1489	1483	1477	1465
					1463	1437	1438		
									1395
1370	1371	1373	1373	1375	1378	1378	1375	1379	1382
1342									
1321	1320	1322	1321	1322		1326	1320	1323	1323
1297	1286	1290	1288		1298	1292	1288		
1249	1257	1262	1268	1269	1250	1267	1262	1264	1268
					1184	1184			
1130					1129	1133	1143	1136	1130
1091	1098	1097	1099	1100	1090				
1013	993	994	996	1005	1015	1004	989	1001	1009
942	950	951	957		942	953			972
922	912	913	909	916	924	910		915	
	798	796	798	809		811	816	811	805
737	749	762	759	744	767				
697					698	720	725		729
627	626				627	624	626		
					590				
	560	561		555		558	541	562	550
484	494	496	491	498	508	491	492	493	499
457	472	469	474	477	479	472			
447	454	453	453	455	444	452	455	451	449
	432	434						433	
396	394	393	373	397		391	359		
	318	320	316	320					
295	284	284			293	300	304	300	
	234	239	232	241	232	229	230	242	231

hypericin or the chromophore spectrum. Overall, the low frequency regions are quite distinctive for each of the two compounds.

Resonance Raman (RR) spectra were also obtained for the free stentorin chromophore and are shown in Figure 7. The intensity of the RR spectra is much weaker than that of the SERRS spectra of the stentorin chromophore (Figures 3b and 5b), and some relative intensity differences are observed, however most band positions are similar. For the RR 458 nm spectrum, the largest change (compared to the SERRS spectrum) is the decreased relative intensity of the 1292 cm^{-1} band. In the RR 568 nm spectrum, the relative intensity of the 1258 cm^{-1} band is much larger and the 1285 cm^{-1} band is less defined. The low frequency regions (not shown) of the RR spectra for both excitation wavelengths were very weak and featureless. The use of SERRS allowed many of the weak low frequency bands to be observed.

The stentorin chromophore spectra are quite similar to those of the stentorin protein complexes but there are also some differences. The high frequency regions of the stentorin I spectra are almost identical to those of the free chromophore, with the exception of a few small frequency shifts. The low frequency region is also quite similar, but some relative intensity differences as well as some peak broadening in the stentorin I spectra are observed. The peak broadening is most evident in the 750-850 cm^{-1} and the 900-1000 cm^{-1} regions.

Several differences between the free chromophore spectra and those of stentorin II and IIB are observed. The 1292 cm^{-1} chromophore band has virtually disappeared in the 458 nm spectra of both the stentorin II complexes and the corresponding band in the 568

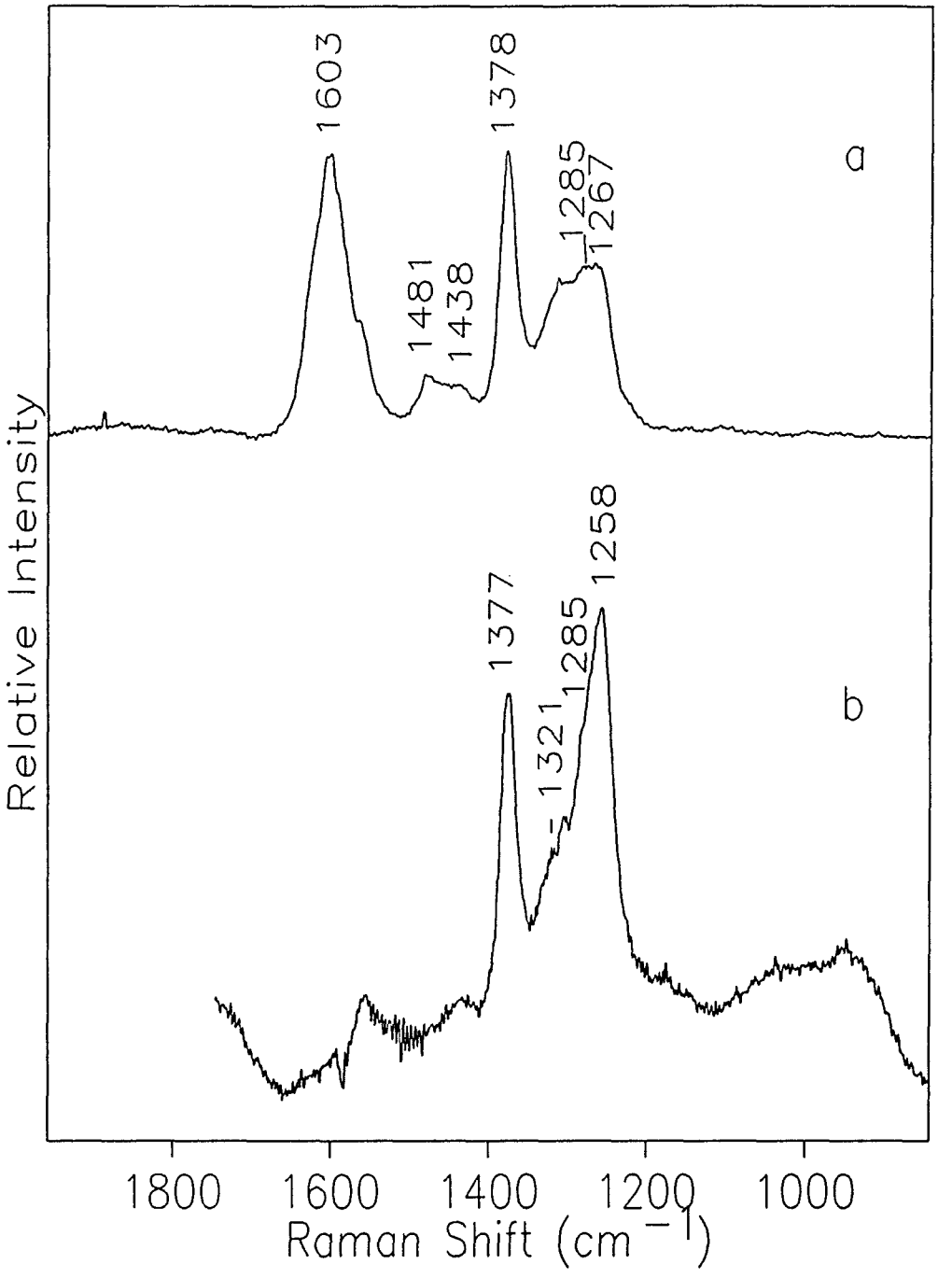

Figure 7. Resonance Raman spectra of stentorin chromophore film obtained with a) 458 nm excitation and b) 568 nm excitation. Laser power at the sample was 10 mW. Integration time 100 s.

nm spectra is drastically decreased. In the 568 nm high frequency spectra of the stentorin IIs, the relative intensity of the 1642 cm^{-1} and 1549 cm^{-1} bands is increased and the 1269 cm^{-1} band is shifted from 1257 cm^{-1} in the free chromophore. The high frequency region of stentorin IIB differs from the chromophore in several other respects. The most obvious are the large increase in the relative intensity of the 1551 cm^{-1} shoulder in the 458 nm spectrum and the appearance of a new shoulder at 1395 cm^{-1}. The low frequency spectra for the stentorin IIs are harder to analyze due to the much lower signal intensity that was obtained for these compounds. However some differences from the chromophore are observed. The low frequency spectra for both stentorin II complexes exhibit the same broad backgrounds in the 750-850 cm^{-1} and 900-1000 cm^{-1} regions that are observed in the stentorin I spectra. Also, as with stentorin I, the relative intensity of the bands between 390-500 cm^{-1} are different from those of the free chromophore. The 300 cm^{-1} band is also much less intense in the stentorin II spectra.

Discussion

Unfortunately, the complexity of the hypericin structure makes it impossible to completely assign all of the vibrational modes without a normal coordinate analysis. However, Raser *et al.*[19] have made some tentative band assignments for hypericin. The hypericin band at 1370 cm^{-1} has been assigned to the in-plane vibrations of the central fragment that contains the carbonyl groups. The other high frequency bands from 1650 to 1250 cm^{-1} have been assigned as C-C stretching modes of the four "corner" benzene fragments. Bands from 1160 to 1100 cm^{-1} are C-CH in-plane bending vibrations and the bands between 1030 and 680 cm^{-1} are due to in-plane bending modes.[19-21] In addition the

bands in the 550 to 400 cm^{-1} region are likely due to out-of-plane bending of the benzene corner fragments.[22] Although these vibrational assignments are very general, useful information about the stentorin compounds can still be obtained.

A comparison of the stentorin and hypericin spectra provides structural information about the stentorin chromophore as well as additional support for the Raman band assignments. The hypericin 1370 cm^{-1} band has been tentatively assigned to the in-plane vibration of the central carbonyl containing fragment. Since stentorin has the same structure as hypericin through this section of the molecule, the corresponding stentorin band should be located at the same frequency as the hypericin band. This appears to be the case in both the 458 nm and the 568 nm spectra. The high frequency bands from 1650 to 1250 cm^{-1} are assigned to C-C stretching modes of the outer benzene fragments of the four corner rings. These band positions as well as their relative intensities should be affected by different substituents on the benzene rings. Most of the stentorin bands in this high frequency region exhibit changes in their relative intensities and/or are shifted from the corresponding hypericin bands. These ring stretching modes can be shifted to either higher or lower frequencies depending upon the exact nature of the vibration. Although the differences in the two high frequency spectra can easily be accounted for by structural differences, such relative intensity changes and frequency shifts may also be observed as a result of different orientations of the two compounds on the SERRS substrate. In addition, strong interactions of an adsorbate with a metal surface can also cause relative intensity changes and frequency shifts. However, the resonance Raman and SERRS spectra of hypericin have been compared and are very similar, indicating that

hypericin only interacts weakly with the silver substrate[19]. The structural similarity of stentorin makes it probable that stentorin would also interact weakly with the silver surface. The similarity of the resonance Raman spectra of stentorin to the SERRS spectra further support a weak interaction of the stentorin with the silver surface. The decreased relative intensity of the 1286 cm^{-1} band in the RR spectra of the stentorin chromophore is also observed for the corresponding band in the hypericin RR spectra. This mode may be enhanced because of the orientation of the hypericin/stentorin at the surface. From the high frequency region alone, it is difficult to discern whether orientation and/or structural effects are responsible for the spectral differences.

The low frequency regions for the stentorin chromophore and hypericin are quite distinctive from each other. Both spectra have several bands in common, which again indicates a structural similarity between the two compounds. Also, as in the high frequency region, band shifts and relative intensity changes occur. The bands in the 550 to 400 cm^{-1} region are out-of-plane bending modes of the benzene fragments. These modes are sensitive to ring substituents because they can interact with the out-of-plane bending vibrations of the ring substituents[22]. Therefore the band shifts and relative intensity changes seen in this region are reasonable considering the structures of the two compounds. The unique bands in the two spectra could be the result of either orientation or structural effects. However, it is unlikely that an orientation effect alone would produce such similar shaped spectra in the high frequency region and such different spectra in the low frequency region. It therefore seems reasonable that most of the changes observed between the hypericin and the chromophore spectra are the result of

their structural differences. There may be some orientation effects, but they appear to be minor.

Comparison of the SERRS spectra of the stentorin free chromophore to stentorin I, stentorin II and stentorin IIB furnishes information about the chromophore of these protein complexes. Since it was necessary to acid denature the stentorin complexes, little information concerning the native protein-chromophore interactions can be deduced. The higher relative intensity of the bands around 1640 cm^{-1} and 1550 cm^{-1} is likely an orientation effect. The interaction of the chromophore with the polypeptide chain of the surrounding protein matrix may prevent the chromophore from adsorbing to the SERRS surface in the same orientation as the free chromophore. The high frequency region of the stentorin II complexes are similar to the RR spectra of the free chromophore. The similarities include the decreased intensity of the 1288 cm^{-1} band in both excitation spectra, and the increased relative intensity if the 1269 cm^{-1} band in the 568 nm excitation spectra. The fact that the stentorin II spectra appear more like the RR spectra of the free chromophore than the SERRS spectra of the free chromophore can again be attributed to an orientation effect caused by an incomplete denaturation of the surrounding protein matrix. The high frequency differences in the 458 nm stentorin IIB spectrum can also be explained as a result of incomplete denaturation. The 1395 cm^{-1} band could be the result of the interaction of amino acid residues with the central carbonyl fragment of the chromophore. The large 1551 cm^{-1} band may either be the result of a protein interaction or an orientation effect. The low frequency regions are actually quite similar to that of the free chromophore. The band broadening and

background effects observed in the low frequency region of stentorin complexes are likely the result of the buffer and acid components of the protein dipping solutions. Both of these degrade the silver surface and can produce impurity bands in this region. In addition, denaturation of the protein complexes can produce inhomogeneity in the samples which also causes band broadening.

Most of the differences between the protein SERRS spectra and those of the free chromophore can be explained as a result of either orientation effects or protein interactions. These differences are actually fairly minor and it would appear from these results that the chromophore of all three protein complexes (stentorin I, stentorin II and stentorin IIB) is the same. Overall the spectra are very similar to those of the free chromophore.

Conclusions

The use of SERRS spectroscopy has proven to be a sensitive diagnostic tool for the study of chromophore-containing proteins. The fluorescence of the stentorin chromophore was effectively quenched by the silver substrate for all systems studied. The SERRS spectra of the stentorin chromophore confirm that the structure of stentorin is very similar to hypericin and both molecules interact weakly with the silver surface. However, spectra obtained in the low frequency region demonstrate the capability of SERRS spectroscopy to differentiate between two structurally similar molecules. In addition this study indicates that the structure of the chromophore in all three protein complexes (stentorin I, stentorin II and stentorin IIB) is very closely related or identical. This suggests that any functional differences between stentorin I and stentorin II are the

result of environmental effects rather than chromophoric differences.

Acknowledgements

This work was supported by grants from the National Institute of Health (GM35108 TMC and NS15426 to PSS) and the Army Research Office (28748-LS-SM to PSS)

References

(1) Song, P. S.; Häder, D. P.; Poff, K. L. *Photochem. Photobiol.* **1980,** *32,* 781.

(2) Song, P. S.;Häder, D. P.; Poff, K. L. Poff *Arch. Microbiol.* **1980,** *126,* 181.

(3) Walker, E. B.; Lee, T. Y.; Song, P.-S. *Biochim. Biophys. Acta,* **1979,** *587,* 129.

(4) Lankester, M. A. *Q. J. Microsc. Sci.* **1873,** *13,* 139.

(5) Møller, K. M. *C. R. Trav. Lab. Carlsburg* **1962,** *32,* 471.

(6) Wood, D. C. *Photochem. Photobiol.* **1976,** *24,* 261.

(7) Tao, N.; Orlando, M.; Hyon, J. S.; Gross, M.; Song, P.-S. *J. Amer. Chem. Soc.* **1993,** *115,* 2526.

(8) Kim, I. H.; Rhee, J.; Huh, J.;Florell, S.; Faure, B.; Lee, K.; Kahsai, T.; Song, P.-S.; Tamai, N.;Yamazaki, T.;Yamazaki, I. Biochim. Biophys. Acta **1990,** *1040,* 43.

(9) Song, P. S.; Kim, I.; Florell, S.; Tamai, N.; Yamazaki, T.; Yamazaki, I. *Biochim. Biophys. Acta* **1990,** *1040,* 58.

(10) Savikhin, S., Tao, N., Song, P.-S., Struve, W. S. *J. Phys. Chem.* **1993,** *97,* 12379.

(11) Yamazaki, T., Ohta, N., Yamazaki, I. *J. Phys. Chem.* **1993,** *97,* 7870.

(12) Dai, R. *Ph.D. Dissertation* University of Nebraska, Lincoln, Nebraska, 1994.

(13) Brown, D. W.; Hauser, F. M.; Tommasi, R.; Corlett, S.; Salvo, J.J. *Tetrahedron,* **1993,** *34,* 419.

(14) Nicholson, R. S.; Shain, I. *Anal. Chem.* **1964,** *36,* 706.

(15) Evans, D.H.; O'Connell, K. M.; Petersen, R. A.; Kelly, M. J. *Chem. Ed.* **1983,** *60,* 706.

(16) Bruno, R.; Pham, M. C.; Dubois, J. E. *Electrochim. Acta,* **1977,** *22,* 451.

(17) Redepenning, J.; Tao, N. *Photochem. Photobiol.* **1993,** *58,* 532.

(18) Cotton, T. M. In *Spectroscopy of Surfaces* Clark, R. J.; Hester, R. E. Eds.; John Wiley & Sons: New York, 1988; 91.

(19) Raser, L. N.; Kolaczkowski, S. K.; Cotton, T. M. *Photochem. Photobiol.* **1992,** *56,* 157.

(20) Gastilovich, E. A.; Klimenko, V. G.; Kopteva, T. S.; Migel, I. A.; Shigorin D. N. *Russ. J. Phys. Chem. (Engl. trans.)* **1986,** *60,* 125.

(21) Dutta, P. K.; Hutt, J. A. *J. Raman Spectros.* **1987,** *18,* 339.

(22) Colthup, N. B., L. H. Daly, and Wiberley, S. E. *Introduction to Infrared and Raman Spectroscopy 3rd Edition* Academic Press: Boston, 1990.

LANGMUIR-BLODGETT FILMS OF HYPERICIN

A paper to be submitted to *Langmuir*

Jeanne L. Wynn, Brian W. Gregory, and Therese M. Cotton

Abstract

Monolayer films of hypericin, a photodynamic polycyclic quinone, were prepared at the air-water interface, and were transferred to substrates to form Langmuir-Blodgett (LB) films. These films were investigated using absorption, fluorescence and surface enhanced resonance Raman scattering (SERRS) spectroscopies. Both the spectroscopic data and the π-A isotherms suggest that hypericin forms π-π aggregates that orient vertically to the subphase surface. The effect of subphase on the π-A isotherm was also investigated. The addition of ions to the subphase caused the films at the air-water interface to become less stable, suggesting that hydrogen bonding plays an important role in the stabilization of the monolayers. For an acid subphase, the hypericin was found to orient with a carbonyl in the aqueous phase. Stable monolayers were also prepared on a $FeCl_3$ subphase. However these monolayers did not transfer well.

Introduction

Since the pioneering work of Langmuir and Blodgett, the study of ordered molecular assemblies at the air-water interface has continued to grow at an exponential rate. However most of these monolayer studies have involved long chain lipid based molecules.[1,2] Aromatic molecules often require derivatization with extended non-polar chains in order to form stable monolayers. Several recent studies have expanded the focus of Langmuir-Blodgett films to include compounds that lack long chain aliphatic

tails. Three examples of this are porphyrin derivatives[3-4], anthracene derivatives with short chain substituents[5-6], and rigid rod oligomides[7-9]. Successful deposition of 500 layers of anthracene derivatives with aliphatic side chains as short as four CH_2 units has been reported.[5-6] The formation of stable close-packed layers has also been demonstrated for several polycyclic aromatic quinones.[7-9]

Hypericin is a rigid, polycyclic aromatic quinone (Figure 1) that is known to exhibit a variety of photodynamic effects.[10-13] The current interest in hypericin has centered on its antiviral activity. Hypericin has been shown to be active against several retroviruses including the Friends leukemia virus and the human immunodeficiency virus.[14-15] Several investigations have demonstrated that the presence of light is important for hypericin's antiviral activity.[16-18] Although the mode of action is currently not known, several mechanisms have been proposed. These include singlet oxygen generation, superoxide radical formation, and excited state proton transfer.[19-23] There is evidence that hypericin undergoes all three processes.[20,22,23]

To understand the mechanism of action of hypericin more fully, the relevant chemical and physical parameters must first be established. The preparation of ordered films may be very useful for investigating some of the fundamental properties of hypericin. For instance, polarization studies can be performed on ordered films to determine the polarization of the electronic transitions. Raman excitation profiles may also yield important information regarding the excited state. Another application is the inclusion of hypericin in lipid bilayers in order to emulate the interaction of hypericin with viral envelopes. The focus of this study it to investigate the feasibility of the

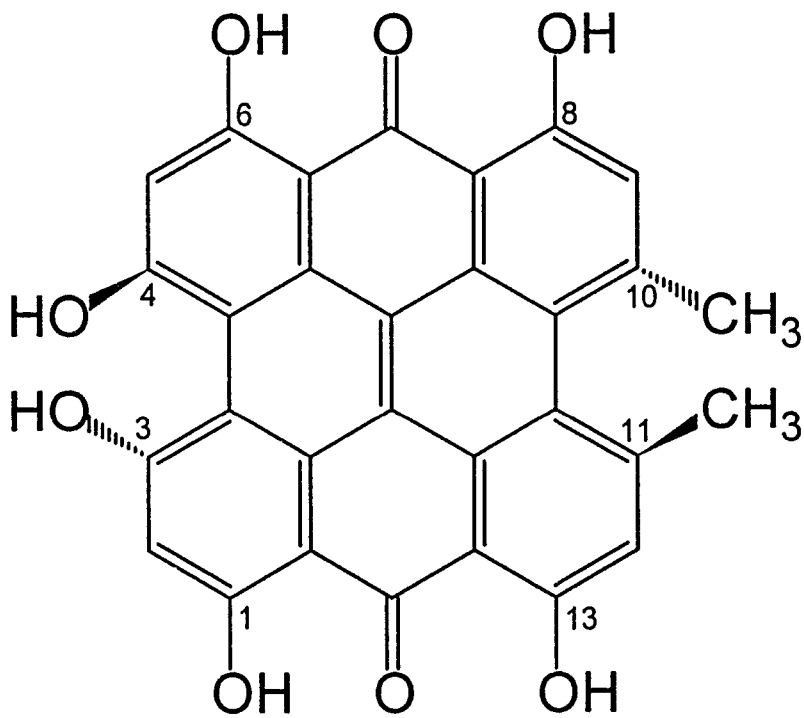

Figure 1. Structure of hypericin.

preparation and transfer of Langmuir-Blodgett films of hypericin to solid substrates.

Experimental

Hypericin was obtained from LC Services Corporation (Woburn, Massachusetts). Ultrapure water was obtained following pretreatment with carbon and particulate filters and reverse osmosis. It was further deionized by a Milli-Q (Millipore Corporation) purification system and had a nominal resistivity of 18 MΩcm. Ferric chloride was obtained from Baker. All other reagents were purchased from Fisher. Methanol and chloroform were both HPLC grade solvents. Chloroform was purified further by passing it through a basic alumina column. All other reagents were used without further purification.

Hypericin was spread from a chloroform/methanol (9:1) solution. The concentration of the spreading solution was determined daily by UV-VIS absorption spectroscopy. An aliquot of the spreading solution was diluted with ethanol, and the concentration was calculated by measuring the absorbance at 590 nm (ε = 41,600 $M^{-1}cm^{-1}$).[24]

Langmuir films of hypericin were formed by spreading 200 µL of a 0.06 mg/mL solution at the air-water interface of a conventional computer controlled teflon Langmuir trough. After an equilibrium period of 30 minutes, the monolayer was compressed at the rate of 7 cm^2/min. Monolayer surface pressure measurements were recorded by differential weight measurements using a filter paper Wilhelmy plate suspended from a microbalance. Monolayer depositions were accomplished by emersion of the substrates through the compressed monolayer film at a surface pressure of 20 mN/m. The transfer rate for the films was 1.6 mm/min and transfer ratios were 1.0 ± 10%.

Glass and quartz slides were used for the monolayer transfer studies. The slides were cleaned first in alcoholic KOH for 4-6 hours, and then chromic acid for a minimum of 12 hours. All substrates were sonicated in ultrapure water before use.

Absorption spectra were obtained with a Perkin Elmer Lambda 6 spectrophotometer. All spectra were measured at a scan rate of 480 nm/min.

Surface enhanced resonance Raman spectra were collected using a Spex Triplemate spectrometer with a Princeton Instruments CCD (model LN1152) detector cooled to -120° C. All spectra were collected in a backscattered geometry and the laser power at the sample was approximately 10 mW. The 458 nm line of a Coherent Ar^+ 200 series laser or the 568 nm line of a Kr^+ 100 series laser were used as the excitation source. The SERRS substrates were vacuum deposited silver island films (50 Å). The films were deposited onto glass slides at the rate of 0.2 Å/s using an Edwards (model 306A) coating system. These were coated with the monolayer films as described above. All SERRS spectra were obtained with the substrates immersed in an optical dewar containing liquid nitrogen.

Results and Discussion

The pressure area isotherms obtained for hypericin were found to be very sensitive to the concentration of the spreading solution. Due to the extremely low solubility of hypericin in pure chloroform, a mixed solvent system must be used. Small amounts of hypericin can be solubilized in chloroform with as little as 0.5% methanol. However, in this system hypericin exists in an aggregated state and its solubility is quite low. Hypericin is monomeric in methanol. In this study a 10% methanol solution was used.

This solvent system was chosen in order to minimize aggregation effects, maximize solubility, and yet maintain the requirements of a suitable spreading solvent. However, even with 10% methanol solution, concentrations greater than ~ 2 x 10^{-4} M were found to contain aggregates. The presence of aggregates was detected in two ways: first, if the spreading solution was allowed to stand, particles precipitated from the solution; second, indication of aggregation was obtained from the pressure-area isotherm. The areas obtained are too small. Figure 2 shows isotherms for two different concentrations of spreading solvents. The 5.27 x 10^{-4} M solution contained aggregates, whereas the 1.24 x 10^{-4} M solution did not. For all the solutions that contained aggregates the molecular areas were less than 30 Å^2/molecule. Although there is a substantial difference in the absorption spectra of monomeric and aggregated hypericin, the presence of aggregates could not be determined with the UV-VIS absorption spectra of the spreading solvent.

A typical isotherm for hypericin on water is shown in Figure 3. Monolayer behavior, as exemplified by the isotherms, was found to be somewhat non reproducible from one experiment to the next. Sometimes the isotherm consisted of a simple curve, whereas other times a plateau at the 10 to 15 mN/m pressure range was observed. The molecular areas obtained by extrapolation back to zero surface pressure were typically near 57 Å^2/molecule ± 3 Å^2, and were fairly reproducible, especially at higher pressures. At 30 mN/m areas were 38 Å^2/molecule ± 1 Å^2. Collapse of the molecular films occurred at pressures near 32 mN/m. The hysteresis behavior observed with consecutive compression/expansion cycles is probably the result of aggregates or strongly associated hypericin molecules that do not dissociate upon expansion.

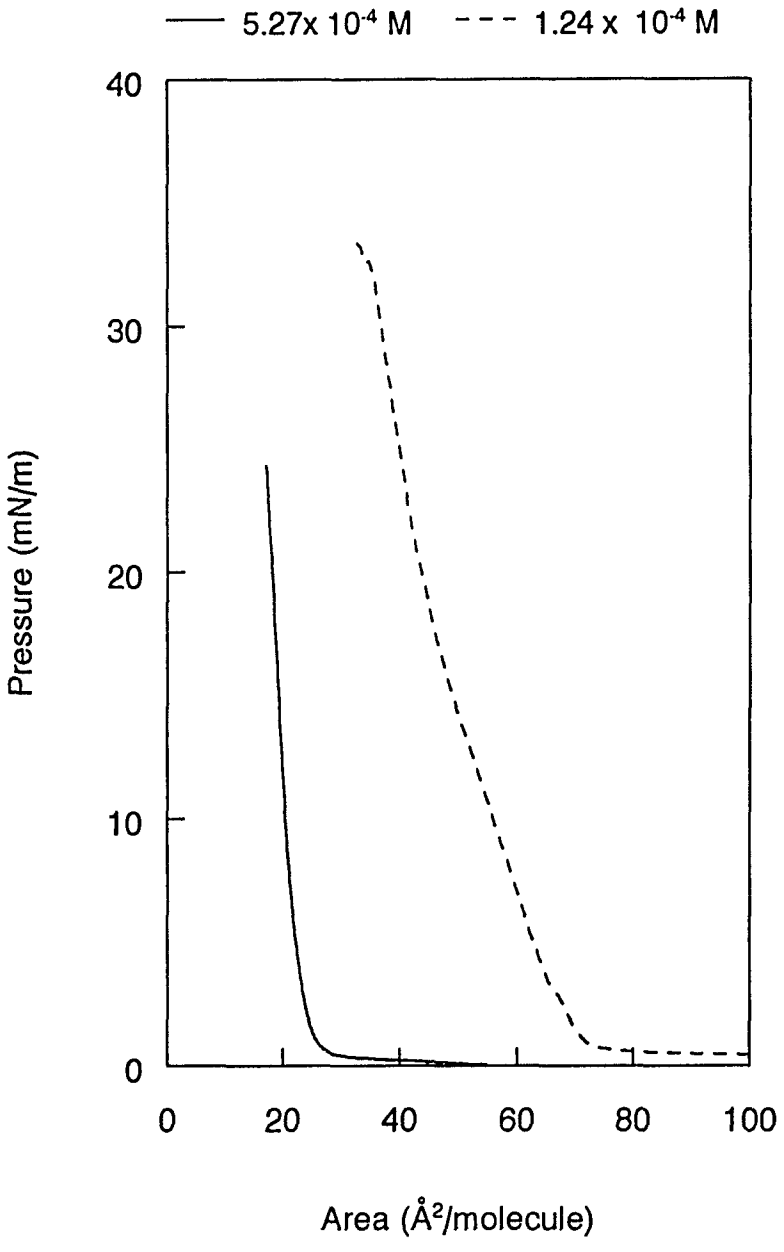

Figure 2. π-A isotherm of hypericin at two spreading solution concentrations. The subphase was water. Both solution were 90% chloroform 10% methanol.

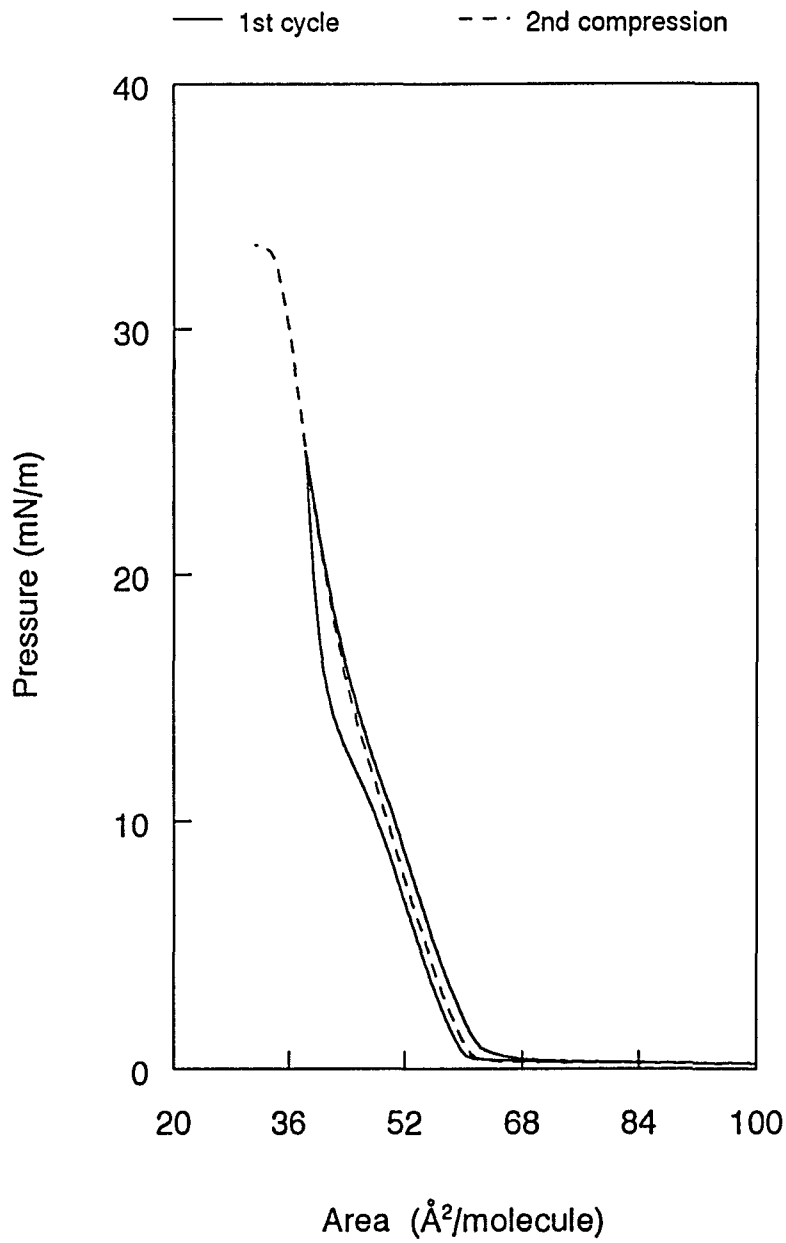

Figure 3. π-A isotherm of hypericin. The subphase was water.

An absorption spectrum of a transferred hypericin film on quartz is shown in Figure 4. For comparison, the absorption spectrum of a dried film is also shown. The two spectra differ in several ways. The redband (605 nm) in the LB monolayer is severely attenuated and has lost all indications of the vibronic peaks (567 nm and 607 nm are vibronic peaks of the S_1 transition of hypericin[25]). Both the 342 nm and the 485 nm bands are redshifted from the corresponding peaks in the dried film spectrum, and the 485 nm band is much more intense. The absorption spectrum of the LB film is indicative of strong interactions between the hypericin molecules. The dry film spectrum is typical of that obtained for hypericin solutions containing aggregates. Yamazaki *et al.*[26] have proposed that these aggregates consist of a lattice structure involving a head-tail hydrogen bonded network and/or some ring stacking. It is apparent from the absorption spectrum that the LB film structure is different from the typical hypericin aggregate structure formed in solution. A possible structure for the LB film will be discussed later.

Surface enhanced resonance Raman spectra (SERRS) were also obtained for the LB films and compared to those adsorbed from solution, and are displayed in Figure 5. The overall spectral intensity for the L-B films was 3-4 times greater than that for the solution adsorbed films. The SERRS spectra for the two types of films are for the most part very similar, with the exception of a few minor band shifts and relative intensity changes.

Due to the complexity of the hypericin molecule, the vibrational modes of the molecule have not been fully assigned. However, Raser *et al.*[27] have made some tentative band assignments which are shown in Table 1. Most of the changes seen in the SERRS

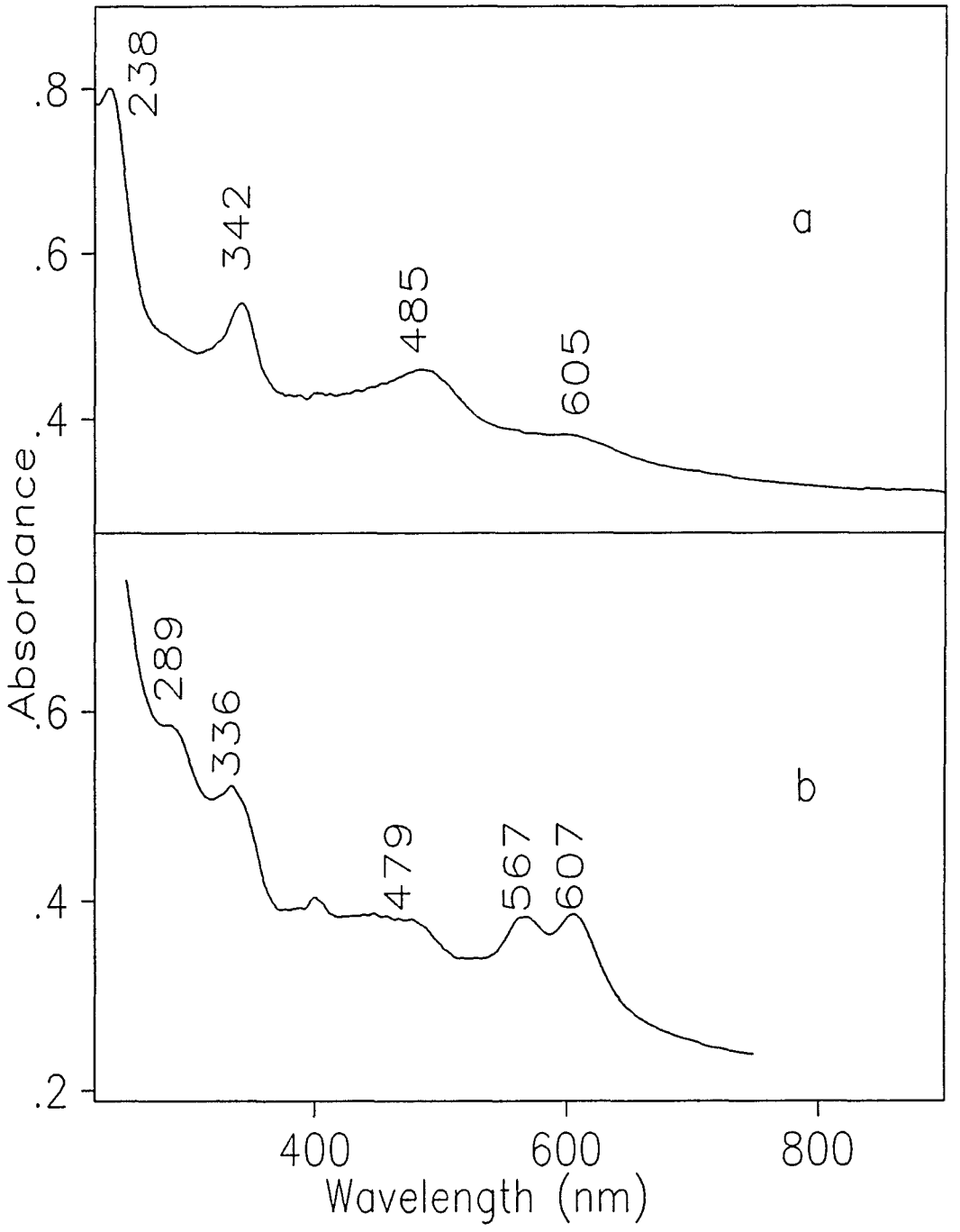

Figure 4. UV-Vis absorption spectra of a) LB film of hypericin transferred to 8 quartz slides b) dried drop of hypericin solution on a quartz slide. Scan speed was 480 nm/min.

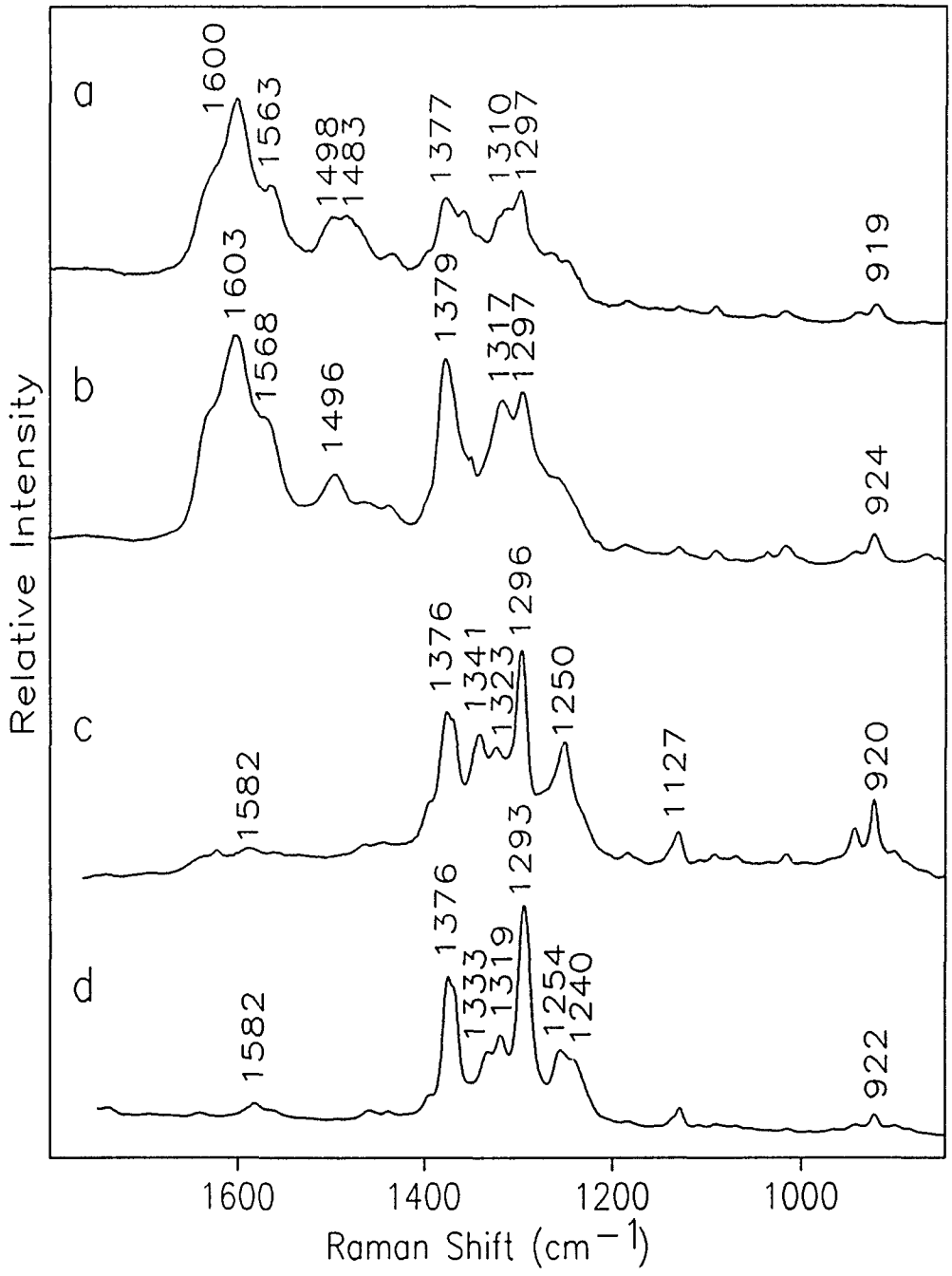

Figure 5. SERRS spectra of hypericin a) solution-adsorbed film at 458 nm excitation, b) LB film at 458 nm excitation, c) solution-adsorbed film at 568 nm excitation, d) LB film at 568 nm excitation. Integration times: a and b 100 s, c and d 60 s. 77 K.

Table 1 Raman band assignments for hypericin

Raman shift (cm^{-1})	Assignment[a]
1650 - 1250	C-C stretch of four "corner" benzene fragments
1634	contribution from non-hydrogen bonded carbonyl[29]
1600	contribution from hydrogen bonded carbonyl[28,29]
1370	in-plane vibration of the central carbonyl containing fragment
1160 - 1100	C-CH in-plane bending
1030 - 680	C-C in plane bending
400 - 550	out of plane bending of benzene ring fragments[30,31]

[a] from reference 27 unless otherwise indicated

spectra for the hypericin films are in the 1650 to 1250 cm^{-1} region (the C-C stretching modes of the corner rings). The largest band shifts are seen in the 568 nm excitation spectra, where the 1341 cm^{-1} band of the self-adsorbed film is shifted to 1333 cm^{-1} in the LB film spectra, and the 1323 cm^{-1} band is shifted to 1318 cm^{-1}. In the LB film, the 1250 cm^{-1} band is split into two bands, one at 1255 cm^{-1} and another at 1242 cm^{-1}. Most of the band positions for the 458 nm excitation spectra are the same for both spectra, although some relative intensity changes are observed. These changes are most notable for the ring bands from 1380 cm^{-1} to 1250 cm^{-1} in the LB film spectrum. The relative intensities are changed both with respect to each other and with respect to the other higher frequency bands. One other notable relative intensity change is in the 940 and 920 cm^{-1} bands of the 568 nm excitation spectra. These bands are much more intense for the self-adsorbed film. The low frequency regions for the two films were found to be almost identical.

Relative intensity changes and minor band shifts observed in SERRS spectra are often indicative of orientational differences. Both the absorption and SERRS spectra demonstrate that at least some degree of ordering that is not present in the normal aggregate lattice structure has been obtained through the use of the Langmuir-Blodgett technique.

The orientation of the hypericin at the air water interface in very difficult to discern. The molecular area of hypericin in the plane of the macrocycle obtained from a space filling CPK model is about 12 Å x 12 Å x 5 Å. The areas obtained from the isotherms suggest that hypericin does not orient in a horizontal fashion at the air-water interface. In

fact, previous studies with polycyclic aromatic ring systems have concluded that ring systems often stack face-to-face at the air-water interface[2,3,7]. Although the minimum area for hypericin oriented vertically is approximately 60 Å^2, the areas obtained on water are probably too small for a single monolayer in this configuration. This suggests that there may be some stacking or aggregation in the hypericin films. Since hypericin is fairly symmetric and there are three sides that could interact with the water subphase it is not possible from the present data to determine the exact orientation of the molecules at the air-water interface. Polarized absorption experiments may help determine the orientation of the hypericin at the air-water interface.

Although the exact orientation of the hypericin molecules at the air-water interface can not be determined at this time, a strong case can be made for a strongly-interacting ring stacked structure that is oriented vertically to the water subphase. Three things support strong interactions between the hypericin molecules in the LB film: 1) the hysteresis observed in the π-A isotherm that was discussed earlier; 2) the strong perturbation of the absorption spectrum; and 3) the LB film was found to be non-fluorescent. Hypericin in a monomeric state is highly fluorescent, but most aggregates are not fluorescent. The differences in absorption spectra suggest that the interactions are not the hydrogen bonded lattice system described earlier. A π-π stacked structure is supported by the areas obtained from the π-A isotherm.

Other subphases were investigated to determine if better monolayers could be obtained. These include: 1 mM phosphate buffer (pH = 6.5), 10 mM phosphate buffer (pH = 6.5), ~10 mM HCl (pH = 1.3), 10 mM NaOH (pH = 11), 10 mM NaCl, and 10

mM $FeCl_3$. The phosphate buffer and NaCl subphases were chosen to determine the effect of ions on the monolayers, whereas the acidic, basic and $FeCl_3$ subphases were selected in an effort to help determine orientations of hypericin at the air-water interface Protons and Fe^{3+} are both known to interact with the carbonyl portions of hypericin[29,32,33], whereas OH^- can deprotonate hypericin at position 3[34]. With the exception of $FeCl_3$, all the other subphases gave less reproducible isotherms than those obtained for a pure water subphase. All isotherms displayed phase transitions in the 10-14 mN/m range; however, the length and slope of the transition varied. The molecular areas were also extremely irreproducible with variations as great as 25%. The single exception was $FeCl_3$.

The isotherm obtained for an $FeCl_3$ subphase is shown in Figure 6. These isotherms were found to be very reproducible with a molecular area of 83 $Å^2$/molecule when extrapolated to zero surface pressure. The area at 30 mN/m was 54 $Å^2$/molecule. This area is somewhat larger than that obtained on a pure water subphase; thus it is possible that hypericin forms a single oriented layer at the air-$FeCl_3$ interface. The collapse pressure for these monolayers was also higher than for the other films. Hypericin is known to chelate to Fe^{3+} through a carbonyl, so it is reasonable to think that possibly hypericin orients with a carbonyl in the water phase.[32,33] Transfers were made of these films onto quartz substrates. Lower transfer ratios (0.4-0.8) were obtained for these films compared to those transferred from other subphases. The band positions in the SERRS spectra (not shown) of the $FeCl_3$ subphase hypericin films were nearly identical to those obtained for the pure water subphase films. However, the spectra for the $FeCl_3$-hypericin films were broader and displayed some relative intensity differences compared to the

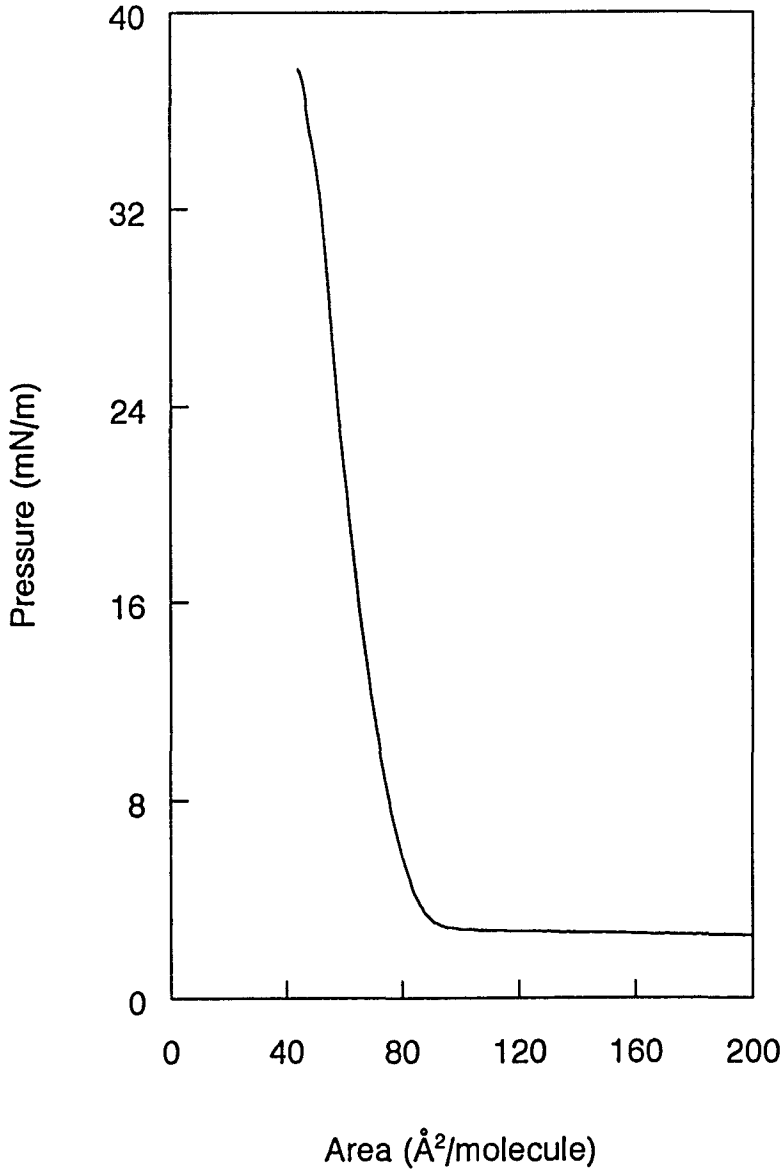

Figure 6. π-A isotherm of hypericin. The subphase was $FeCl_3$.

spectra of the water subphase film. The significance of these results will be discussed later.

Hydrogen bonding is known to play an important role in both the solvation and aggregation of hypericin. Previous studies have shown that the solvatochromatic behavior of hypericin is related to the hydrogen bonding ability of the solvent.[29] In addition, hydrogen bonding is thought to play an important role in the interaction of hypericin molecules with other hypericin molecules in aggregates.[26] Therefore, any interactions of hypericin at the air-water interface probably would also involve hydrogen bonding. This is supported by the irreproducibility of the films on the NaCl and phosphate buffer subphases. The presence of ions in the subphase likely interferes with the hydrogen bonding interactions at the air-water interface causing the films to become less stable and more susceptible to multi-layer formation.

The irreproducibility of the acid and base subphases may also be due to the presence of ions in the subphase, but since hypericin is slightly soluble in these subphases, solubility effects may also play a role in the reproducibility as well. These subphases were studied in an effort to gain orientational information. The SERRS spectra obtained for films transferred from the NaOH subphase were identical to the spectra obtained for those from the water subphase at the same transfer pressure. Two possible explanations for this are: 1) the hypericin did not orient at the air-NaOH interface with the position 3 OH close enough to the surface to be deprotonated; or 2) all of the deprotonated hypericin dissolves into the subphase and is not transferred to the SERRS substrate.

The spectra of the films transferred from the acid subphase were different from those obtained from the aqueous subphase. Their SERRS spectra, along with the spectra of solution adsorbed acidic hypericin (pH = 1), are shown in Figures 7 and 8 for 458 nm excitation. In the presence of acid, hypericin is protonated. For the spontaneously-adsorbed film, there are several indicators of protonation that can be observed in the SERRS spectra. One is the enhancement of the shoulder of the 1603 cm^{-1} peak. This band is thought to contain contributions from the hydrogen-bonded carbonyls of the hypericin[28,29]. When hypericin is protonated, the hydrogen bonding is lost or weakened, which in turn shifts the band to a higher frequency. The band at 1634 cm^{-1} has been assigned to a non-hydrogen-bonded carbonyl of the hypericin.[29] Another indicator of protonation is the large increase in the relative intensity of the 1382 cm^{-1} band. This band has been assigned to the vibration of the central-carbonyl containing fragment of the macrocycle, so some type of change in this band should occur upon protonation of the carbonyl. Indicators of protonation in the low frequency region are the appearance of the band at 964 cm^{-1} and the relative intensity increase in the 586 cm^{-1} band. With the exception of the 964 cm^{-1} band, all of these indicators are also present in the LB film of hypericin transferred from the HCl subphase. The 964 cm^{-1} band may be an effect from the hydrochloric acid added to the dipping solution of the solution-adsorbed film. The similarity in SERRS spectra between the self-adsorbed acidic hypericin solution and the LB acid subphase film suggests that there is some interaction of at least one carbonyl of the hypericin at the acid-air interface.

If Fe^{3+} is chelated to a carbonyl of hypericin in the transferred film, several of the

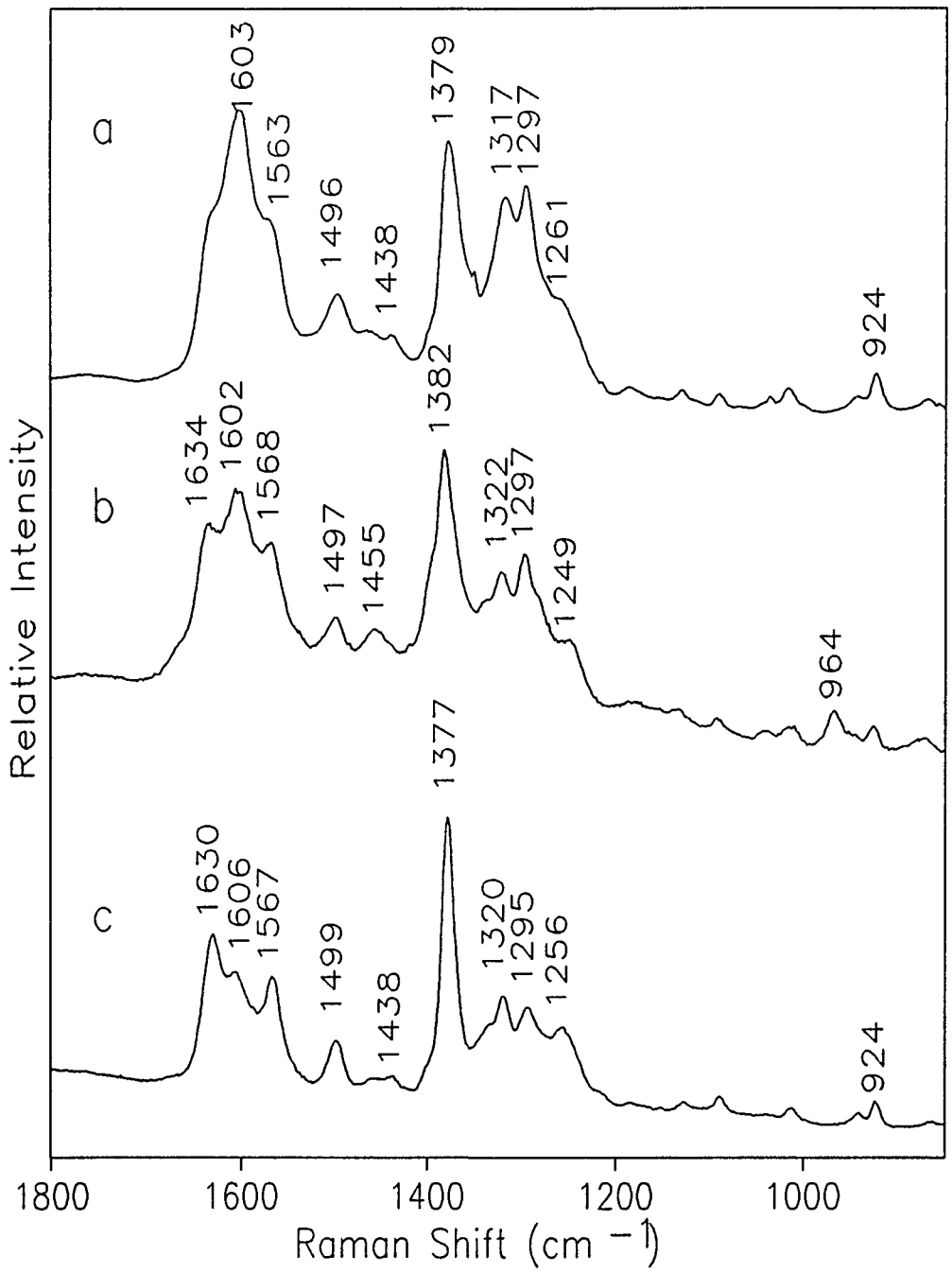

Figure 7. High frequency SERRS spectra of hypericin obtained with 458 nm excitation. a) LB film from water subphase, b) solution-adsorbed film from acidic ethanol (pH = 1) hypericin solution, c) LB film from 10 mM HCl subphase. Integration times were 100 s. 77 K.

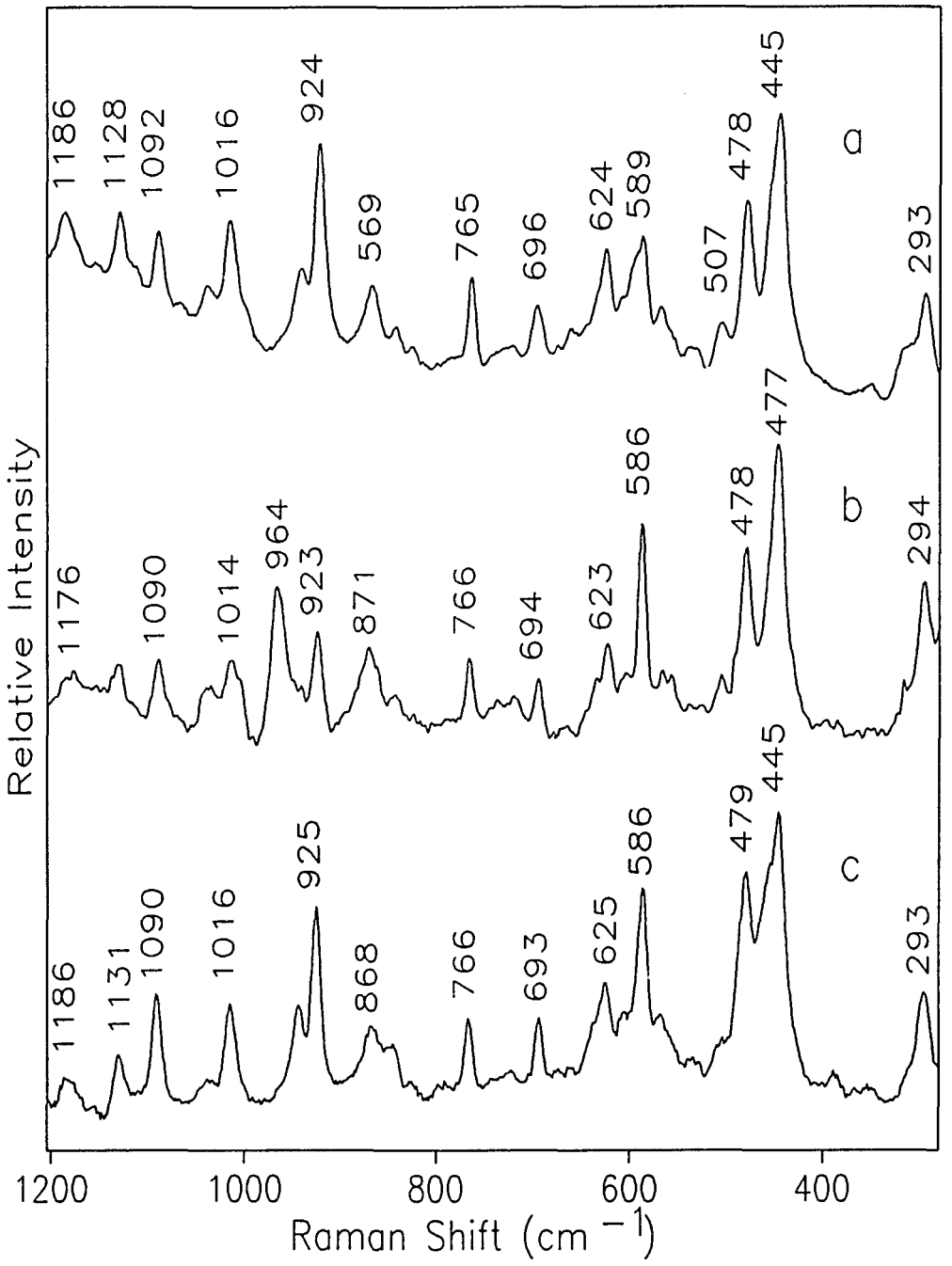

Figure 8. Low frequency SERRS spectra of hypericin obtained with 458 nm excitation. a) LB film from water subphase, b) self-adsorbed film from acidic ethanol (pH = 1) hypericin solution, c) LB film from 10 mM HCl subphase. Integration times were 100 s. 77 K.

same indicators should be observed in the SERRS spectra of the hypericin. The fact that none were observed suggests that the Fe^{3+} does not become incorporated into the transferred films. Although these films were stable at the air-water interface, they do not appear to transfer well. Both the lower transfer ratios and the broader SERRS bands support this. If the films do not maintain their organization upon transfer to quartz substrates, this could cause more disorder in the film and result in band broadening. The hypericin films at the air-$FeCl_3$ interface may be too rigid to transfer well. It is not unusual to find that films of rigid molecules do not transfer well with the vertical deposition method.[9]

Conclusions

Monolayers of hypericin at the air-water interface have been studied by π-A isotherms, and have been transferred to solid supports. The spectroscopic data of the transferred films suggests that the films are at least partially ordered, although the extent is not clear. Both the absorbance and fluorescence spectra suggest that there are strong interactions between the hypericin molecules in the LB films. Molecular areas from the π-A isotherms suggest that the ring systems of hypericin are oriented vertically to the subphase but that some multilayer or aggregation may be experienced in the films. The use of a mixed monolayer system, may help minimize some of this multilayer formation. Hydrogen bonding is also believed to play an important role for the stabilization of the hypericin films at the air-water interface. However, it is not possible from the present data to determine specifically which functional group(s) are involved in these interactions. Polarized absorption measurements may help determine this. From the protonation of the

carbonyl observed in the SERRS spectra, hypericin is thought to orient with one of the carbonyls in the acid subphase. A similar orientation may occur at the $FeCl_3$ subphases, however these films did not transfer well. This may be because of their rigidity.

Acknowledgments

This work was supported by a grant from the National Institute of Health (GM35108 TMC). The authors also wishes to thank Brian Gregory, Jiyu Fang and Jay Y. Wang for their assistance with the monolayers techniques and the helpful discussions.

References

(1) Ulman, A. *An Introduction to Ultrathin Organic Films From Langmuir-Blodgett to Self Assembly,* Academic Press: Boston, 1991.

(2) Roberts, G. *Langmuir-Blodgett Films,* Plenum Press: New York, 1990.

(3) Hahn, R. A.; Gupta, S. K.; Fryer, J. R.; Eyres, B. L. *Thin Solid Films,* **1985,** *134,* 35.

(4) Bull, R. A.; Bulkowski, J. E. *J. Colloid Interface. Sci.* **1983,** *92,* 1.

(5) Vincett, P. S.; Barlow, W. A.; Boyle, F. T.; Finney, J. A. *Thin Solid Films,* **1979,** *60,* 265.

(6) Steven, J. H.; Hahn, W. A.; Barlow, W. A.; Laird, T. *Thin Solid Films,* **1983,** *99,* 71.

(7) Kenny, P. W.; Miller, L. L.; Rak, T. H.; Jozefiak, T. H.; Christopfel, W. C.; Kim, J.-H.; Uphaus, R. A. *J. Am. Chem. Soc.* **1988,** *110,* 4445.

(8) Cammarata, V.; Kolaskie, C. J.; Miller, L. L.; Stallman, B. J. *J. Chem. Soc. Chem. Commun.* **1990,** 1290.

(9) Cammarata, V.; Atanasoska, L.; Miller, L. L; Kolaskie, C. J.; Stallman, B. J. *Langmuir,* **1992,** *8,* 876.

(10) Pace, N.; Mackinney, G. *J. Am. Chem. Soc.* **1941,** *63,* 2570.

(11) Giese, A. C. In *Photophysiology Current Topics in Photobiology and Photochemistry,* Vol VI, Giese, A.C., Ed.; Academic Press: New York, 1971; 77.

(12) Knox, J. P.; Dodge, A. D. *Plant Cell Environ.* **1985,** *8,* 19.

(13) Durán, N.; Song, P.-S. *Photochem. Photobiol.* **1986,** *43,* 677.

(14) Meruelo, D.; Lavie, G.; Lavie, D. *Proc. Natl. Acad. Sci. USA* **1988,** *85,* 5230.

(15) Lavie, G.; Valentine, F.; Levin, B.; Mazur, Y.; Gallo, G.; Lavie, D.; Weiner, D.; Meruelo, D. *Proc. Natl. Acad. Sci. USA* **1989,** *86,* 5963.

(16) Carpenter, S.; Kraus, G. A. *Photochem. Photobiol.* **1991,** *53,* 169.

(17) Hudson, J. B.; Lopez-Bazzocchi, I.; Towers, G. H. N. *Antivir. Res.* **1991,** *15,* 101.

(18) Lopez-Bazzocchi, I.; Hudson, J. B.; Towers, G. H. N. *Photochem. Photobiol.* **1991,** *54,* 95.

(19) Heitz, J. R. In *Light Activated Pesticides,* Heitz, J. R.; Downum, K. R., Eds.; American Chemical Society: Washington D.C., 1987; 38.

(20) Knox, J. P.; Samuels, R. I.; Dodge, A. D. In *Light Activated Pesticides,* Heitz J. R.; Downum, K. R., Eds.; American Chemical Society: Washington DC, 1987; 265.

(21) Gai, F.; Fehr, M. J.; Petrich, J. W. *J. Am. Chem. Soc.* **1993,** *115,* 3384.

(22) Gai, F.; Fehr, M. H.; Petrich, J. W. *J. Phys. Chem.* **1994,** *98,* 5784.

(23) Weiner, L.; Mazur, Y. *J. Chem. Soc. Perkin Trans. 2* **1992,** 1439.

(24) Scheibe, G.; Schöntag, A. *Chem. Ber.* **1942,** *75,* 2019.

(25) Jardon, P.; Lazortchak, N.; Gautron, R. *J. Chim. Phys. Phys-Chim. Biol.* **1987,** *84,* 1141.

(26) Yamazaki, T.; Nobuhiro, O.; Yamazaki, I.; Song, P.-S. *J. Phys. Chem.* **1993,** *97,* 7870.

(27) Raser, L. N.; Kolaczkowski, S. V.; Cotton, T. M. *Photochem. Photobiol.* **1992,** *56,* 157.

(28) Tao, N.; Orlando, M.; Hyon, J.-S.; Gross, M.; Song, P.-S. *J. Am. Chem. Soc.* **1993,** *115,* 2526.

(29) Wynn, J. L.; Cotton, T. M. *J. Phys. Chem.* **1994,** submitted

(30) Wynn, J. L.; Kim, J.-H.; Ningbing, T.; Dai, R.; Song, P.-S.; Cotton, T. M. *Photochem. Photobiol.* **1994,** submitted.

(31) Colthup, N. B.; Daly, L. H.; Wiberley, S. E. *Introduction to Infrared and Raman Spectroscopy 3rd Edition,* Academic Press: Boston, 1990.

(32) Golard, A. G.; Brody, S. S. In *NATO ASI Series Vol H15, Photosensitisation,* Moreno, G. Ed. Springer-Verlag: Berlin, 1988, 63.

(33) Jardon, P.; Nafis, M. *J. Chim. Phys.* **1994,** *91,* 99.

(34) Falk, H.; Meyer, J.; Oberreiter, M. *Monatsh. Chem.* **1992,** *123,* 277.

GENERAL SUMMARY

The absorption and fluorescence spectra of hypericin in solution were examined in order to determine the aggregation states of hypericin. Hypericin was found to be monomeric in most polar organic solvents, and to be aggregated in non-polar solvents and in water. An understanding of the aggregation state of hypericin is necessary in order to determine the mechanism of action for photodynamic anti-viral activity of hypericin. The mechanism and/or the anti-viral activity of hypericin may be dependent upon its aggregation state. Surface enhanced resonance Raman spectroscopy was also employed to confirm the assignment of the polarization of the electronic transitions. Knowledge of which electronic transitions are involved in the photodynamic action of hypericin is important to elucidate structural reactivity of the molecule.

The vibrational spectra of the chromophore for three *Stentor* protein complexes (stentorin I, stentorin II and stentorin IIB) were compared using surface enhanced resonance Raman spectroscopy. The chromophore for each protein complex produces the same spectra. This suggests that the chromophore is the same and that the functional differences between the protein complexes is the result of the surrounding protein environment of the chromophore rather than differences in the chromophore itself.

Ordered films of hypericin can be prepared and transferred using the Langmuir-Blodgett technique. The extent of order in the films as well as the orientation of the hypericins is unknown at this time. The stability of the films is affected by the presence of ions in the subphase.

The work presented in this dissertation establishes the groundwork for possible

future experiments. There are several possibilities for future monolayer experiments. First, a mixed-monolayer system, where hypericin is mixed in a lipid matrix, should be investigated. This may produce a more stable monolayer system, as well as reducing aggregation effects in the films. A system of hypericin incorporated into a mixed monolayer where hypericin-hypericin interaction are minimized, would provide an ideal system for Raman excitation profiles. This may yield important information regarding the excited state. Mixed monolayer system would also be useful as membrane models for investigating virus-hypericin interactions. Polarization studies of hypericin films, both at the air-water interface and transferred to solid substrates, are necessary to determine the orientation of the hypericin in the films.

Another potential area for future study is the use of normal coordinate analysis to assign specific vibrations of the hypericin molecule. In addition to being very helpful for the Raman studies of hypericin, they may be useful for determining the exact structure of the stentorin chromophore. This work would be done in collaboration with Dr. Pill-Soon Song at the University of Nebraska.

ACKNOWLEDGEMENTS

There are many people I wish to thank for making my time at Iowa State worthwhile. Dr. Cotton: thank you for your support and encouragement during five years here. I have really enjoyed being in your group and getting to know you. I would also like to acknowledge all the members of the Cotton group, both past and present. Each of you have made my time here more enjoyable. Lana: thanks for showing me the ropes when I first joined the group. Lydia: you have become a very dear friend, whom I will cherish forever. Joe: many days were more enjoyable just because of your presence. Steve: thank you for your friendship and guidance. Both you and Joe have taught me so much more than just chemistry. The months we spent building the spectrometer will always be one of my favorite time here at Iowa State. Jae-Ho: thanks for being both a mentor and a friend, even after you left Iowa State. John: it has indeed been a rare privilege getting to know you as a brother in Christ. Al: You truly are a friend that can always be counted on. Thanks for all your help with all the safety stuff. Morgan: I have really enjoyed our many discussions. Brian, Jay Y., Hung, Cheng-Li, Fang, George, Kostia and Brian C.: thanks for all the great volleyball games. I shall miss them. I have enjoyed working with and getting to know each of you.

Finally I wish to thank my parents who have always supported me in all of my endeavors.